© 2023. Published by The Company of Biologists Ltd | Development (2023) 150, dev201497. doi:10.1242/dev.201497

RESEARCH ARTICLE

DOT1L promotes spermatid differentiation by regulating expression of genes required for histone-to-protamine replacement

Aushaq B. Malla[1,*], Shannon R. Rainsford[1], Zachary D. Smith[1,2] and Bluma J. Lesch[1,3,4,*]

ABSTRACT

Unique chromatin remodeling factors orchestrate dramatic changes in nuclear morphology during differentiation of the mature sperm head. A crucial step in this process is histone-to-protamine exchange, which must be executed correctly to avoid sperm DNA damage, embryonic lethality and male sterility. Here, we define an essential role for the histone methyltransferase DOT1L in the histone-to-protamine transition. We show that DOT1L is abundantly expressed in mouse meiotic and postmeiotic germ cells, and that methylation of histone H3 lysine 79 (H3K79), the modification catalyzed by DOT1L, is enriched in developing spermatids in the initial stages of histone replacement. Elongating spermatids lacking DOT1L fail to fully replace histones and exhibit aberrant protamine recruitment, resulting in deformed sperm heads and male sterility. Loss of DOT1L results in transcriptional dysregulation coinciding with the onset of histone replacement and affecting genes required for histone-to-protamine exchange. DOT1L also deposits H3K79me2 and promotes accumulation of elongating RNA Polymerase II at the testis-specific bromodomain gene *Brdt*. Together, our results indicate that DOT1L is an important mediator of transcription during spermatid differentiation and an indispensable regulator of male fertility.

KEY WORDS: Spermiogenesis, Fertility, Histone, Chromatin, Protamine, DOT1L

INTRODUCTION

Mammalian spermatogenesis is a complex developmental process during which male germ cells undergo a series of tightly regulated molecular events to produce mature gametes capable of fertilizing the oocyte. These events include establishment of a spermatogonial stem cell pool, mitotic proliferation, meiosis and morphogenesis of haploid germ cells to produce spermatozoa. The last phase of this process, called spermiogenesis, involves complex biochemical and nuclear morphological transformations that eventually result in acrosome formation, sperm tail biogenesis, sperm DNA condensation and cytoplasm exclusion (Leblond and Clermont, 1952; Oakberg, 1956; Hermo et al., 2010). Although many of the molecular effectors of spermiogenesis have been identified, the gene regulatory factors responsible for their coordination are not well defined.

Spermiogenesis converts the spherical products of meiosis, called round spermatids, into elongated spermatids with the unique nuclear shape typical of mature sperm. This morphological change requires condensation of the spermatid nucleus and is accomplished by enormous chromatin remodeling. During this process, nucleosomes first incorporate histone variants, including TH2B and H2A.L.2, which promote loading of transition proteins TNP1 and TNP2 onto chromatin; the transition proteins promote recruitment and processing of protamines PRM1 and PRM2, and histones and transition proteins are eventually evicted, leaving protamines as the primary packaging protein in a condensed sperm genome (Meistrich et al., 2003; Lewis et al., 2003; Barral et al., 2017; Govin et al., 2007; Merges et al., 2022). This histone-to-protamine transition drastically reduces the sperm nuclear volume, and results in a compact and hydrodynamic nucleus that is resistant to DNA damaging agents, protecting the heritable genome during fertilization (Brewer et al., 1999; Oliva, 2006). Defects in the histone-to-protamine transition produce sperm with abnormal condensation, altered morphology and reduced motility, ultimately leading to failures in fertilization (Cho et al., 2001; Li et al., 2014; Wang et al., 2019; Okada et al., 2007; Shirley et al., 2004; Zhao et al., 2004a,b). How this crucial developmental event is regulated is therefore a fundamental question in reproduction and development.

Several factors important for regulating the histone-to-protamine transition are known. An essential prerequisite for histone removal in elongating spermatids is hyperacetylation of histone H4 (Hazzouri et al., 2000; Morinière et al., 2009; Meistrich et al., 1992; Qian et al., 2013). Acetylation occurs at multiple positions on the H4 protein and helps to loosen sperm chromatin by destabilizing its higher order structure. H4 hyperacetylation requires the histone acetyltransferases GCN5 and EPC/TIP60, recruitment of p300 by the nuclear protein NUT, and activity of the chromatin remodeler CHD5 along with other remodeling complexes (Morinière et al., 2009; Dong et al., 2017; Shiota et al., 2018; Qian et al., 2013; Gaucher et al., 2010; Luense et al., 2019; Li et al., 2014; Zhuang et al., 2014). A key reader of acetylH4 is bromodomain testis-specific protein (BRDT), which binds to acetylated lysines 5 and 8 of H4 (H4K5ac and H4K8ac) through its bromodomain and facilitates acetylH4 eviction and subsequent protamine recruitment (Dhar et al., 2012; Pivot-Pajot et al., 2003; Morinière et al., 2009; Sasaki et al., 2009; Gaucher et al., 2012). Mice specifically lacking the bromodomain of BRDT exhibit defects in histone removal and sperm head elongation due to altered acetylH4 binding (Gaucher et al., 2012; Goudarzi et al., 2016; Shang et al., 2007; Berkovits and Wolgemuth, 2011).

[1]Department of Genetics, Yale School of Medicine, New Haven, CT 06510, USA. [2]Yale Stem Cell Center, New Haven, CT 06510, USA. [3]Department of Obstetrics, Gynecology & Reproductive Sciences, Yale School of Medicine, New Haven, CT 06510, USA. [4]Yale Cancer Center, Yale School of Medicine, New Haven, CT 06510, USA.

*Authors for correspondence (aushaq.malla@yale.edu; bluma.lesch@yale.edu)

Z.D.S., 0000-0002-9283-1957; B.J.L., 0000-0002-6689-0240

Handling Editor: Swathi Arur
Received 30 November 2022; Accepted 20 March 2023

Development (2023) 150, dev201497. doi:10.1242/dev.201497

An underexplored candidate regulator of the histone-to-protamine transition is the histone methyltransferase DOT1L (disruptor of telomeric silencing 1-like, also called KMT4). DOT1L catalyzes mono-, di- and tri-methylation of histone H3 at lysine 79 (H3K79me1/2/3), and these modifications are enriched in meiotic and postmeiotic stages of spermatogenesis, peaking immediately before the histone-to-protamine transition (Ontoso et al., 2013; Dottermusch-Heidel et al., 2014; Feng et al., 2002; Lacoste et al., 2002; van Leeuwen et al., 2002; Ng et al., 2002). In humans, DOT1L is more strongly expressed in testis than in any somatic tissue (Mele et al., 2015; Thul et al., 2017; Uhlén et al., 2015), implying that it has an important role in spermatogenesis. In cell lines, H3K79me and DOT1L promote transcription by binding to RNA polymerase II and its associated protein complexes (Guenther et al., 2008; Steger et al., 2008; Jonkers et al., 2014; Kim et al., 2012; Mohan et al., 2010; Veloso et al., 2014; Wood et al., 2018). H3K79me3 has also been implicated in heterochromatin regulation and was recently shown to be essential for driving major satellite expression, heterochromatin maintenance and chromosomal integrity in mouse embryonic stem cells (Jones et al., 2008; Malla et al., 2021preprint; Ooga et al., 2013). In mice, DOT1L is important for maintenance of spermatogonial stem cell pools (Lin et al., 2022). However, the reported enrichment of H3K79 methylation in late meiosis raises the possibility that DOT1L could also be regulating meiotic and postmeiotic germ cell development.

Here, we investigate the role of DOT1L in spermiogenesis and demonstrate that DOT1L has an important role in histone-to-protamine replacement and in chromatin condensation during sperm differentiation. Specifically, DOT1L positively regulates expression of transition protein and protamine genes, as well as the acetylH4 chaperone gene *Brdt*. Loss of DOT1L in spermatogenic cells leads to defects in the histone-to-protamine transition and is incompatible with fertility, helping to explain why males lacking germline DOT1L are sterile, despite incomplete penetrance of the previously reported spermatogonial stem cell phenotype. Together, our results indicate that DOT1L is a crucial mediator of transcription in spermatids and an indispensable regulator of haploid germ cell differentiation.

RESULTS

DOT1L is highly expressed and H3K79 methylation is enriched in meiotic and postmeiotic germ cells

DOT1L is broadly expressed in a variety of tissues, but is especially abundant in testis (Mele et al., 2015; Papatheodorou et al., 2020; Fonseca et al., 2014; Thul et al., 2017; Uhlén et al., 2015). To identify the precise testicular cell types that express DOT1L, we performed immunofluorescence in wild-type testis cross-sections after validating DOT1L antibody specificity in *Dot1l* knockout testis (see below for conditional knockout strategy and validation). We detected DOT1L expression in most testicular cells, including both germ and somatic cells, with the exception of late post-meiotic cells (elongated spermatids) (Fig. 1A). DOT1L was most highly expressed in nuclei of late pachytene spermatocytes, secondary spermatocytes and round spermatids (Fig. 1B), suggesting a possible requirement in meiotic and postmeiotic stages of spermatogenesis.

As DOT1L is a histone H3 lysine 79 (H3K79) methyltransferase, we next assessed the dynamics of the DOT1L-deposited modifications H3K79me2 and H3K79me3 in meiotic and postmeiotic male germ cells using immunofluorescence in chromosome spreads (Fig. 1C-E). Consistent with previous results in other cell types (Ontoso et al., 2013; Malla et al., 2021 preprint; Ooga et al., 2008), H3K79me2 was present throughout the euchromatin but excluded from DAPI-dense heterochromatin in pachytene spermatocytes and round spermatids, while H3K79me3 was strongly enriched in heterochromatin but mostly depleted from euchromatin (Fig. 1C,D). In elongating spermatids, H3K79me2 was broadly present throughout the chromatin, while H3K79me3 was present in restricted DAPI-dense domains that were reminiscent of chromocenters, which are the DAPI-dense heterochromatic structures composed primarily of pericentromeric repeats (Fig. 1E). These results suggest that DOT1L is active during meiotic and postmeiotic stages of spermatogenesis, and imply that it may be important for either meiotic division or postmeiotic spermatid differentiation.

Germ cell-specific deletion of DOT1L causes male infertility in mice

To evaluate the function of DOT1L in spermatogenesis, we generated a germ cell conditional knockout for *Dot1l* (*Dot1l* cKO) by crossing mice carrying a conditional *Dot1l* allele (Dot1l$^{f/f}$) (Bernt et al., 2011) with mice carrying a *Ddx4-Cre* transgene (Gallardo et al., 2007; Hu et al., 2013) (Fig. 2A). *Ddx4-Cre* is expressed in prenatal germ cells beginning by embryonic day 15.5 and mediates recombination of target alleles by birth (Gallardo et al., 2007; Hu et al., 2013). DOT1L protein expression was completely abolished in *Dot1l* cKO adult testis (Fig. 2B). *Dot1l* cKO males produced no offspring after mating with wild-type females for 6 months (Fig. 2C), indicating that DOT1L is required for male fertility. Testes of young adult 3-month-old *Dot1l* cKO mice were reduced in size compared with control mice but did not display any gross morphological defects (Fig. 2D). Epididymides of *Dot1l* cKO mice were mostly devoid of mature sperm and instead contained abnormally condensed and round cells (Fig. 2E). DAPI staining of germ cells isolated from the cauda epididymis of *Dot1l* cKO and control mice confirmed that the small number of sperm-like cells in the epididymides exhibited abnormal elongation and condensation in the *Dot1l* cKO, compared with normal sperm head morphology in control animals (Fig. 2F). The abnormally elongated sperm in *Dot1l* cKO epididymis contained fragmented DNA detected by TUNEL staining, suggesting that they have undergone apoptosis (Fig. 2G). These findings demonstrate that loss of DOT1L in spermatogenic cells produces defective sperm with decondensed chromatin, depletes the number of normal sperm in the epididymis and ultimately causes infertility.

DOT1L loss causes defects in postmeiotic spermatid differentiation

We next performed histological analysis of Hematoxylin and Eosin stained testes of control and *Dot1l* cKO mice in order to more precisely dissect the role of DOT1L in sperm formation. We observed that *Dot1l* cKO testis exhibited two types of seminiferous tubules. About 25% of tubules displayed a Sertoli cell-only phenotype devoid of any germ cells, indicative of defective spermatogonial stem cell proliferation, as recently reported (Lin et al., 2022). However, most tubules possessed both meiotic and postmeiotic germ cells, indicating successful completion of meiosis (Fig. 3A,B). Immunostaining for DDX4 (also known as MVH), a marker for meiotic and postmeiotic germ cells, revealed that 65% of tubules in our *Dot1l* cKO contained MVH positive germ cells (Fig. 3C,D). At tubule stages X and I, which are distinguished by presence of late pachytene spermatocytes and elongating spermatids

Development (2023) 150, dev201497. doi:10.1242/dev.201497

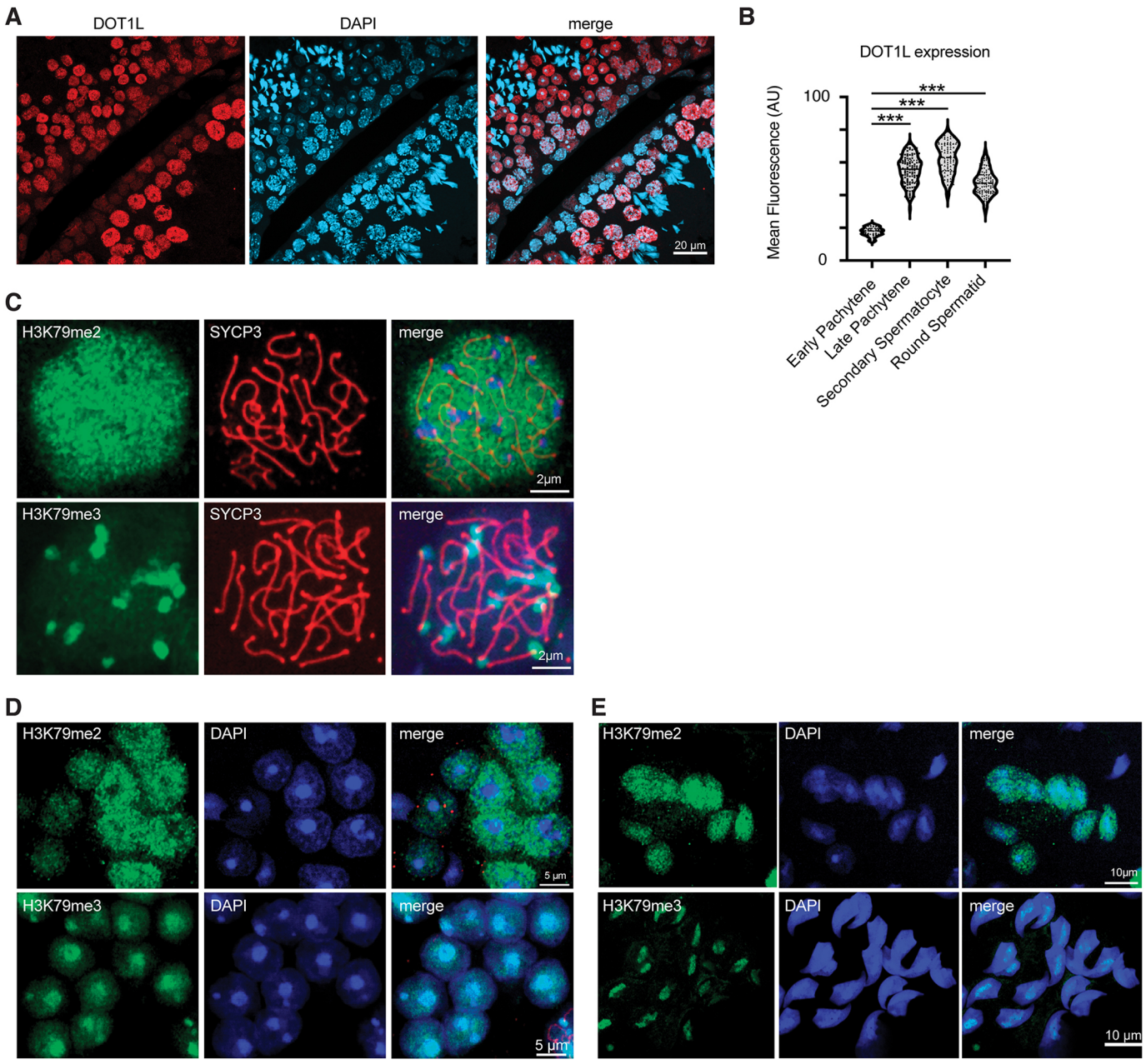

Fig. 1. DOT1L and H3K79 methylation are enriched in meiotic and postmeiotic germ cells. (A) Immunostaining of DOT1L (red) in 3-month-old wild-type testis. DNA is counterstained with DAPI (light blue). Scale bar: 20 µm. (B) Quantification of DOT1L expression in *n*=2 wild-type mice for early pachytene spermatocytes (*n*=50), late pachytene spermatocytes (*n*=102), secondary spermatocytes (*n*=81) and round spermatids (*n*=110). ***P<0.0001 (unpaired two-tailed *t*-test). (C) Immunostaining of surface spreads of primary spermatocytes from control testes with H3K79me2 (green, top row) or H3K79me3 (green, bottom row), and synaptonemal complex protein 3, SYCP3 (red). DNA was counterstained with DAPI (blue). Scale bars: 2 µm. (D,E) Immunostaining of surface spreads of round spermatids (D) and elongating spermatids (E) from wild-type testes with H3K79me2 (green, top row) or H3K79me3 (green, bottom row). DNA was counterstained with DAPI (blue). Scale bars: 5 µm in D; 10 µm in E.

(stage X), or by early pachytene spermatocytes, round spermatids and early condensing spermatids (stage I), there were no apparent differences in the composition and arrangement of testicular cells between *Dot1l* cKO and control (Fig. S1). However, *Dot1l* cKO stage VII and VIII tubules, which should contain spermatids in the final stages of maturation (stage VII) or sperm just released into the lumen (stage VIII), were deficient in fully formed elongated spermatids, although early stage elongating spermatids could be seen (Fig. 3A, Fig. S1). Some tubules that should contain elongating or condensing spermatids were missing these cells altogether, and tubules that did contain elongating spermatids displayed both normally and abnormally condensed spermatids (Fig. 3A, Fig. S1). These results indicate that the previously reported defect in spermatogonial stem cell proliferation does not fully explain the completely penetrant male infertility we observe following loss of DOT1L in male germ cells. Instead, our data suggest that infertility is also due to abnormal spermiogenic differentiation of round to elongated spermatids.

To test whether there is any delay in the formation of round spermatids, we collected testis from juvenile control and *Dot1l* cKO

Development (2023) 150, dev201497. doi:10.1242/dev.201497

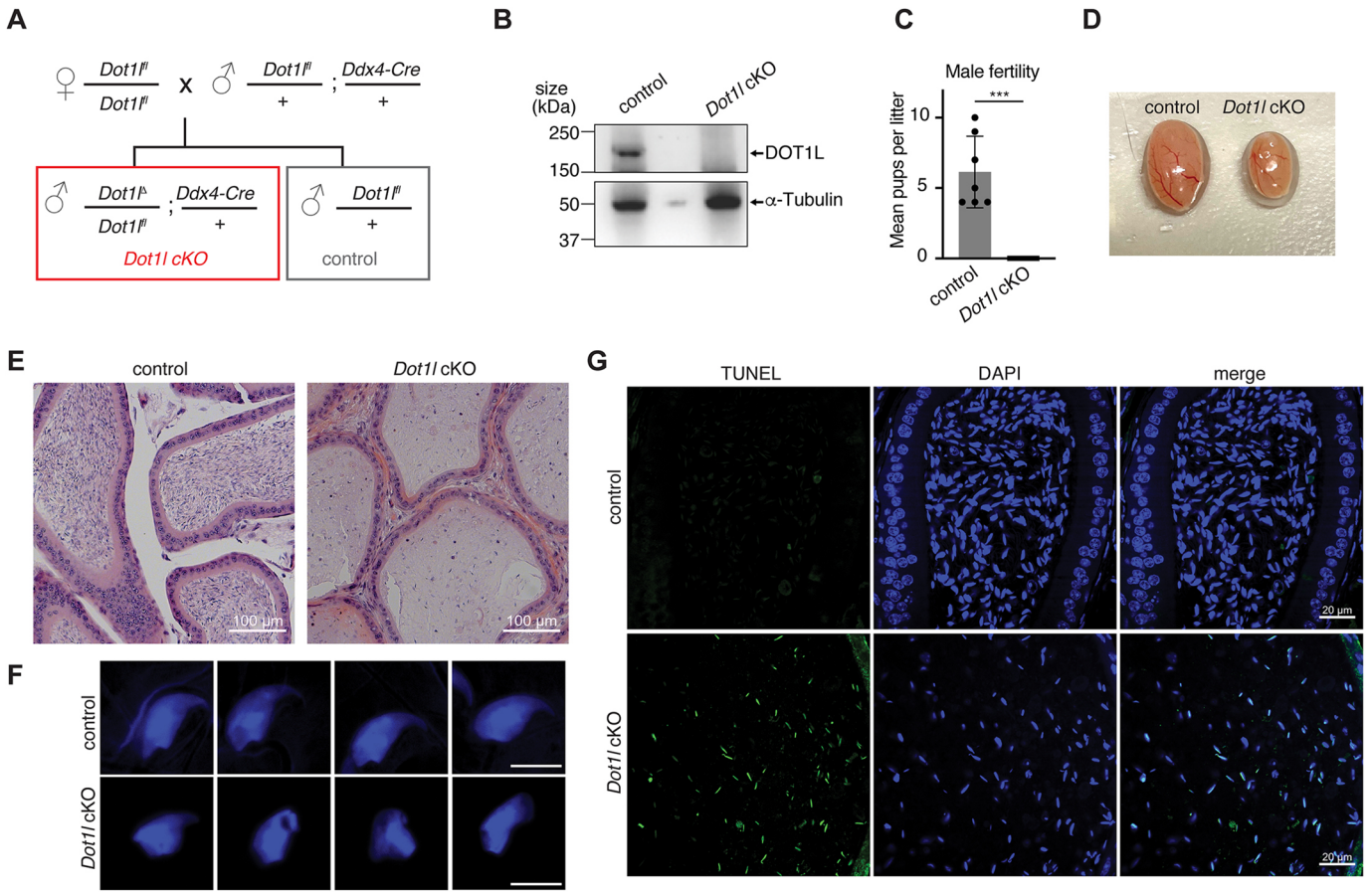

Fig. 2. Germ cell-specific deletion of *Dot1l* leads to male sterility. (A) Schematic for the generation of conditional knockout of *Dot1l* using *Ddx4-Cre*. (B) Western blot for DOT1L in testes of adult control (*Dot1l*$^{fl/+}$*; Cre*−) and *Dot1l* cKO (*Dot1l*$^{fl/\Delta}$*; Cre*+) mice. α-Tubulin serves as a loading control. (C) Number of pups per litter produced by control and *Dot1l* cKO male mice when paired with a wild-type female for 6 months. *n*=7 mice of each genotype; each point represents mean pups per litter for one male. Data are mean±s.d. ***$P \leq 0.0001$ (two-tailed unpaired *t*-test). (D) Gross images of testes from control and *Dot1l* cKO mice. (E) Hematoxylin and Eosin stained epididymal cross-sections of adult control and *Dot1l* cKO mice. Scale bars: 100 µm. (F) DAPI-stained germ cells isolated from cauda epididymides of control and *Dot1l* cKO mice. Scale bars: 5 µm. (G) TUNEL staining (green) in control and *Dot1l* cKO epididymides. DNA was counterstained with DAPI (blue). Scale bars: 20 µm.

mice at 25 days post partum (dpp), when spermatogenesis has progressed to the round spermatid stage but elongating spermatids are not yet present, and performed histological and flow cytometric analysis. Consistent with our results from adult testes, we did not observe any histological differences in composition and arrangement of germ cells in tubules containing postmeiotic cells (Fig. 3E). Similarly, flow cytometry analysis based on DNA content in isolated testicular cells showed similar fractions of cells corresponding to haploid round spermatids (1C), diploid spermatogonia and somatic cells (2C), and tetraploid primary spermatocytes (4C) (Fig. 3F,G), indicating that the defect occurs after the round spermatid stage.

Loss of DOT1L leads to abnormal sperm head elongation and condensation

The known function of DOT1L as a chromatin regulator in combination with our data indicating a role for DOT1L in spermiogenesis suggest that DOT1L might participate in the chromatin condensation that is a central aspect of spermiogenesis (Brewer et al., 1999; Pogany et al., 1981; Zhao et al., 2004b; Ribas-Maynou et al., 2022). Mouse spermiogenesis is divided into 16 steps of spermatid differentiation (1-16) encompassing the major cellular changes of sperm differentiation, including acrosome formation, mitochondrial biogenesis, sperm tail formation and sperm head elongation and condensation (Russell et al., 1990). Sperm head condensation specifically begins at step 9 (corresponding to tubule stage IX) and is complete by step 13 (tubule stage I). To determine the steps of spermiogenesis during which DOT1L is most active, we performed immunostaining for H3K79me2 in wild-type adult testis sections. We analyzed tubules corresponding to stage VIII that have just released mature sperm into the tubule lumen (spermiation), stages IX-XI containing elongating spermatids that are undergoing the histone-to-protamine transition, and stage XII tubules that contain condensing spermatids. We observed intense staining of H3K79me2 in steps 9-11 (tubule stage IX-XI) elongating spermatids, implying high activity of DOT1L at the stages during which sperm-specific chromatin remodeling and condensation take place (Fig. 4A-D). As expected, H3K79me2 was completely absent in step 12 (tubule stage XII) condensing spermatids of control mice because histone removal is complete at this stage (Fig. 4E). H3K79me2 was absent in stage XI tubules of *Dot1l* cKO testes, confirming the specificity of the H3K79me2 antibody (Fig. 4F). These results support a role for DOT1L in regulating sperm head condensation.

To demonstrate the effect of loss of DOT1L on sperm head morphology, we then performed transillumination-assisted

Development (2023) 150, dev201497. doi:10.1242/dev.201497

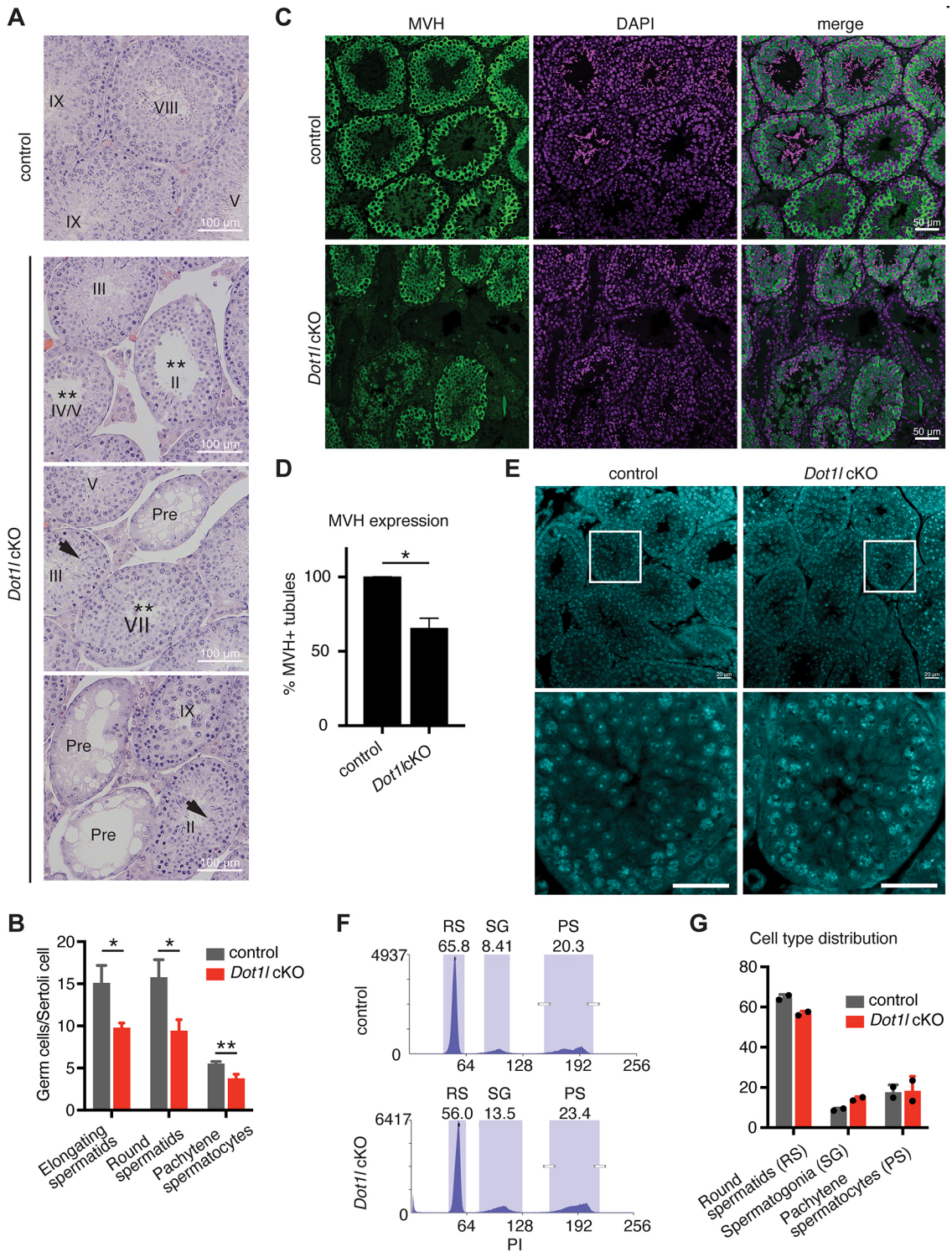

Fig. 3. DOT1L loss causes premeiotic and post-meiotic spermatogenic defects in mice. (A) Hematoxylin and Eosin stained testis cross-sections of control (*Dot1l*$^{fl/+}$; *Cre*−) and *Dot1l* cKO (*Dot1l*$^{fl/\Delta}$; *Cre*+) mice. 'Pre' indicates tubule with pre-meiotic defect; ** indicates loss of elongated spermatids; arrows indicate abnormally condensed elongated spermatids. Scale bars: 100 µm. (B) Quantification of indicated cell types normalized to Sertoli cell number in Hematoxylin and Eosin stained testis cross-sections of control and *Dot1l* cKO mice, as shown in A. *n*=3 tubules corresponding to each stage from *n*=2 mice of each genotype were counted. Data are mean±s.e.m. *$P \leq 0.05$, **$P \leq 0.001$ (two-tailed unpaired *t*-test). (C) Immunostaining of MVH (DDX4) in control and *Dot1l* cKO testis cross-sections. Tubules with no MVH staining in *Dot1l* cKO testis correspond to Sertoli cell-only tubules. DNA is stained with DAPI (magenta). Scale bars: 50 µm. (D) Quantification of MVH-positive tubules as shown in C. Data are mean±s.d. for *n*=2 replicates. *$P<0.05$ (two-tailed unpaired *t*-test). (E) DAPI-stained cross-sections of 25 days post partum (dpp) control and *Dot1l* cKO testis. Scale bars: 20 µm (top panels). Lower panels show increased magnification of tubules outlined in upper panels. Scale bars: 20 µm (bottom panels). (F) Flow cytometry histograms of propidium iodide (PI)-stained testicular cells from dissociated 25 dpp control and *Dot1l* cKO testes showing populations with 1C DNA content (round spermatids, RS), 2C DNA content (spermatogonia, secondary spermatocytes and Sertoli cells, SG) and 4C DNA content (primary spermatocytes, PS). Data are representative of *n*=2 independent experiments. (G) Quantification of relative percentages of cell types in F. Data are mean±s.d. for *n*=2 experiments.

Development (2023) 150, dev201497. doi:10.1242/dev.201497

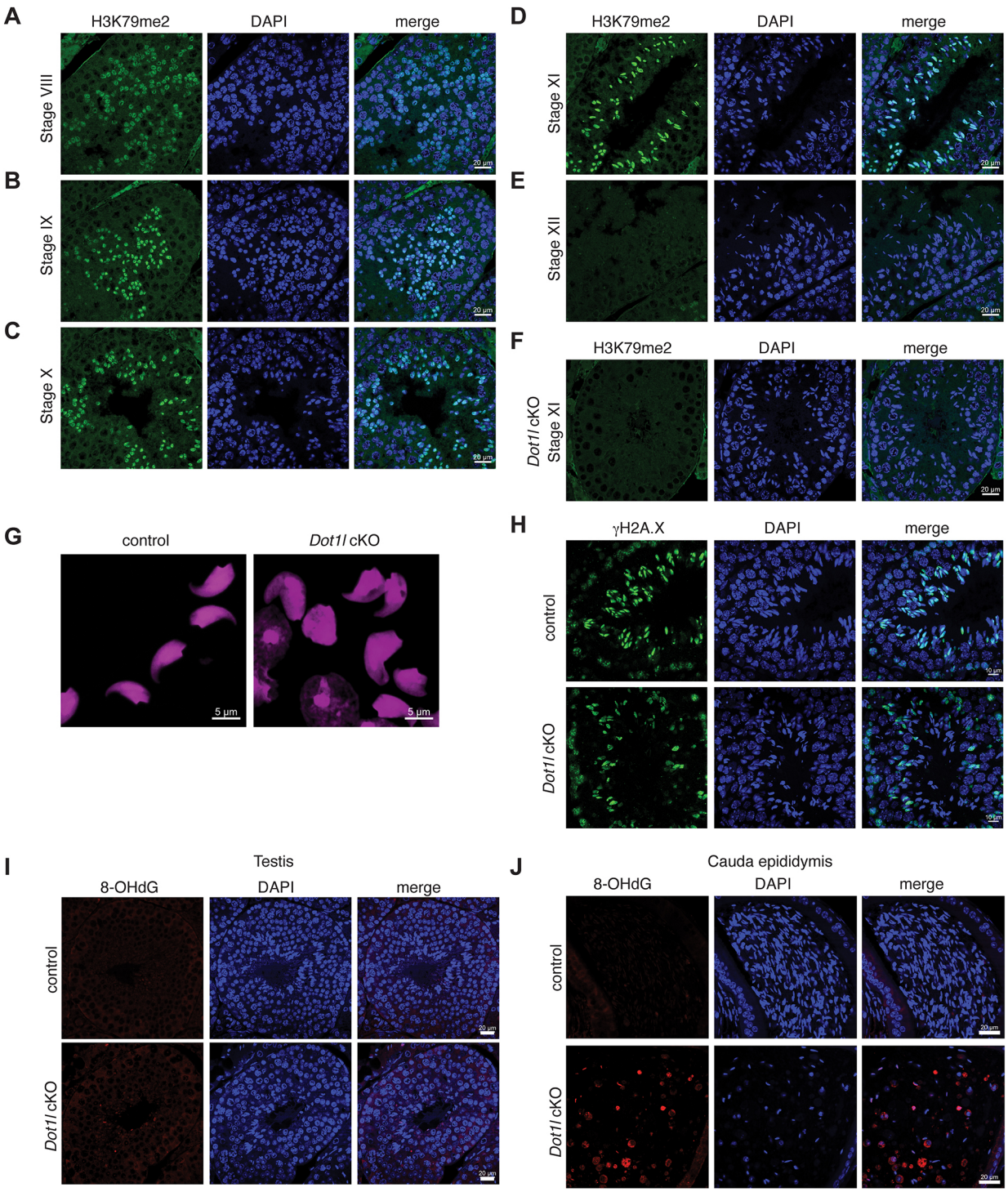

Fig. 4. Loss of DOT1L leads to abnormalities in spermatid elongation and condensation. (A-F) Immunofluorescence for H3K79me2 in control (*Dot1l*$^{fl/+}$; *Cre*−) adult testis cross-sections, showing detectable H379me2 in stage VIII (post-release) early elongating spermatids (A), high enrichment in stages IX-XI elongating spermatids that are undergoing chromatin remodeling (B-D), and complete loss in condensing spermatids after histone replacement at stage XII (E). (F) *Dot1l* cKO (*Dot1l*$^{fl/\Delta}$; *Cre*+) testis stage XI tubules are negative for H3K79me2. Scale bars: 20 µm. (G) Nuclear morphology of elongated spermatids isolated from dark zone regions of seminiferous tubules of control and *Dot1l* cKO mice, and stained with DAPI (magenta). Scale bars: 5 µm. (H) Immunofluorescence for γH2AX (green) in stage X tubule cross-sections of control and *Dot1l* cKO testes. DNA is stained with DAPI (blue). Scale bars: 10 µm. (I) Immunofluorescence for 8-OHdG (red) in testis sections of control and *Dot1l* cKO mice. DNA is stained with DAPI (blue). Scale bars: 20 µm. (J) Immunofluorescence for 8-OHdG (red) in epididymal sections of control and *Dot1l* cKO mice. DNA is stained with DAPI (blue). Scale bars: 20 µm.

microdissection of tubules containing step 13-16 elongated spermatids and stained with DAPI to determine their nuclear shape. Compared with control spermatids, *Dot1l* cKO spermatids exhibited large, poorly condensed nuclei with shapes that were distinct from the typical comma-shaped spermatid nuclei of control mice (Fig. 4G). Although it is possible that the developmental changes occurring in *Dot1l* cKO testes could alter the cell populations recovered from transillumination-based

Development (2023) 150, dev201497. doi:10.1242/dev.201497

microdissection, the shapes observed did not correspond to normal spermatid morphology at any stage (Oakberg, 1956), indicating a defect in sperm head morphogenesis. Mis-shapen sperm heads could arise either due to problems with nuclear condensation or due to defective DNA damage signaling, which is required for histone eviction immediately before chromatin condensation (Leduc et al., 2008; Meyer et al., 2017). Because DOT1L has been implicated in DNA damage repair (Wood et al., 2018; Kari et al., 2019), we tested the levels of DNA damage in *Dot1l* cKO spermatids by staining for the DNA damage marker γH2AX. We observed no difference in γH2AX staining between *Dot1l* and control spermatids, making it unlikely that defects in DNA damage induction explain the head shape defect we observe in *Dot1l* cKO spermatids (Fig. 4H). Further supporting this conclusion, 8-OHdG, a marker of oxidative damage, was occasionally but rarely detected in *Dot1l* cKO testicular germ cells (Fig. 4I), but was elevated in germ cells isolated from the caput epididymis (Fig. 4J), consistent with elevated DNA damage occurring after the onset of nuclear condensation defects.

DOT1L regulates key events of the histone-to-protamine transition in elongating spermatids

One of the central events of mammalian spermiogenesis is the histone-to-protamine transition. During this drastic remodeling event, the histone variant H2A.L.2 is incorporated into chromatin and enables loading of transition proteins (TNP1 and TNP2), which in turn drive recruitment and processing of protamine proteins (PRM1 and PRM2) (Barral et al., 2017; Meistrich et al., 2003; Lewis et al., 2003; Govin et al., 2007; Merges et al., 2022; Hazzouri et al., 2000). Eventually, histones and transition proteins are evicted, resulting in protaminated, hyper-compact sperm chromatin (Meistrich et al., 2003; Lewis et al., 2003; Qian et al., 2013). As *Dot1l* cKO spermatids appeared to exhibit chromatin condensation defects (Fig. 4G), we evaluated the possibility that the histone-to-protamine transition was disrupted in the absence of DOT1L. We assessed the presence of histone H3 in *Dot1l* cKO compared with control seminiferous tubules using immunofluorescence. H3 was observed in stage X elongating spermatids of both control and *Dot1l* cKO mice, as expected (Fig. 5A). However, although histone H3 was no longer detected in elongated spermatids of control mice at stage II, after the replacement of histones by protamines should be complete, H3 persisted in stage II spermatids of *Dot1l* cKO mice (Fig. 5B,C, arrow), pointing to incomplete histone eviction in the *Dot1l* cKO spermatids.

We next evaluated whether protamine loading was also defective by performing immunostaining for PRM1 in squash preparations of control and *Dot1l* cKO elongated spermatids. Compared with control spermatids that exhibited strong PRM1 signal and were normally condensed into a comma shape, *Dot1l* cKO spermatids isolated from testes displayed a variety of abnormalities in PRM1 recruitment (Fig. 5D). The majority (>50%) of *Dot1l* cKO spermatids showed reduced PRM1 staining intensity, whereas another 30% showed high intensity but abnormal localization of PRM1 in the cytoplasm. In the remaining 20% of *Dot1l* cKO spermatids, PRM1 recruitment appeared similar to control (Fig. 5D, bottom row). Among sperm-like germ cells isolated from the *Dot1l* cKO epididymis, the majority showed reduced PRM1 intensity, although the range of PRM1 phenotypes observed in testicular spermatids was also evident (Fig. 5E). Together, these data show that loss of DOT1L impairs histone eviction and protamine recruitment in spermatids.

We then asked how DOT1L acts to promote the histone-to-protamine transition and nuclear condensation. As transition proteins are crucial for guiding recruitment and processing of protamines on chromatin (Barral et al., 2017), we next asked whether transition protein expression was disrupted in the absence of DOT1L. Immunofluorescence staining in testis sections revealed that levels of the transition protein TNP1 were drastically reduced in *Dot1l* cKO testes (Fig. 5F), suggesting that loss of DOT1L impairs expression of both transition proteins and protamines. The major upstream event triggering transition protein and protamine loading is hyperacetylation of histone H4 in stage IX-XI elongating spermatids, with subsequent removal of all acetylated H4 as the spermatids progress to stage XII (Hazzouri et al., 2000; Meistrich et al., 1992; Morinière et al., 2009; Sasaki et al., 2009; Qian et al., 2013). Therefore, we next tested whether DOT1L is required for H4 hyperacetylation. We focused on spermatids undergoing this transition, which occurs at steps 9-12 (tubule stages IX-XII), and performed dual immunostaining of acetylated histone H4 (pan acetylH4) and protamine 2 (PRM2) in control and *Dot1l* cKO testis cross-sections. Similar to our observations for PRM1 (Fig. 5G), we observed reduced staining of PRM2 in most *Dot1l* cKO spermatids at all stages with a fraction of spermatids expressing abnormally high but mislocalized staining. As expected, in wild-type testis acetylH4 was detectable only in step 9-11 (tubule stage IX-XI) elongating spermatids, and PRM2 was highly expressed in spermatids beyond steps 12-16 (tubule stage XII) (Fig. 5G, left panel). In *Dot1l* cKO spermatids, acetylH4 was detected at tubule stages X and XI, similar to control, but abnormally retained in stages III-V, when it is absent in wild type (Fig. 5G, right panel). These results indicate that acetylH4 induction is not affected in *Dot1l* cKO mice, but its removal is impaired. Histone retention can lead to DNA fragmentation, and we found that TUNEL staining was more frequently positive in *Dot1l* cKO elongated spermatids compared with control (Fig. 5H), suggesting that histone retention in *Dot1l* cKO sperm might be triggering apoptosis. Together, our results demonstrate that *Dot1l* cKO mice exhibit incomplete histone replacement and abnormal acetylH4 retention in spermatids during chromatin remodeling, which is correlated with elevated apoptosis.

DOT1L acts as transcriptional activator for genes essential for the histone-to-protamine transition

At the molecular level, DOT1L functions as a transcriptional activator by interacting with RNA polymerase II (Pol II) at promoters and promoting transcriptional elongation (Jonkers et al., 2014; Kim et al., 2012; Mohan et al., 2010; Veloso et al., 2014; Wood et al., 2018; Steger et al., 2008). To understand whether its transcriptional activation function contributes to its role in promoting the histone-to-protamine transition, we performed single cell RNA-sequencing (scRNA-seq) on *Dot1l* cKO and heterozygous control testes. After quality filtering, removal of doublets and dead cells, and harmonization of the control and cKO datasets (see Materials and Methods, Fig. S2A-D), we obtained a final dataset comprising 9823 control and 11,172 *Dot1l* cKO cells. Identities were assigned to an initial set of 20 harmonized clusters based on marker genes (Fig. S2E) and followed a continuous trajectory spanning spermatogenic development from spermatogonia to elongating spermatids, along with four populations of testicular somatic cells, similar to published scRNA-seq datasets from mouse testes (Lukassen et al., 2018; Green et al., 2018; Hermann et al., 2018). Four clusters for which high confidence identities could not be assigned were excluded from downstream analysis, leaving a final set of 16 clusters (Fig. 6A, Table S1).

The distribution of cells across clusters was largely similar between control and *Dot1l* cKO datasets (Fig. 6B). The exception

Development (2023) 150, dev201497. doi:10.1242/dev.201497

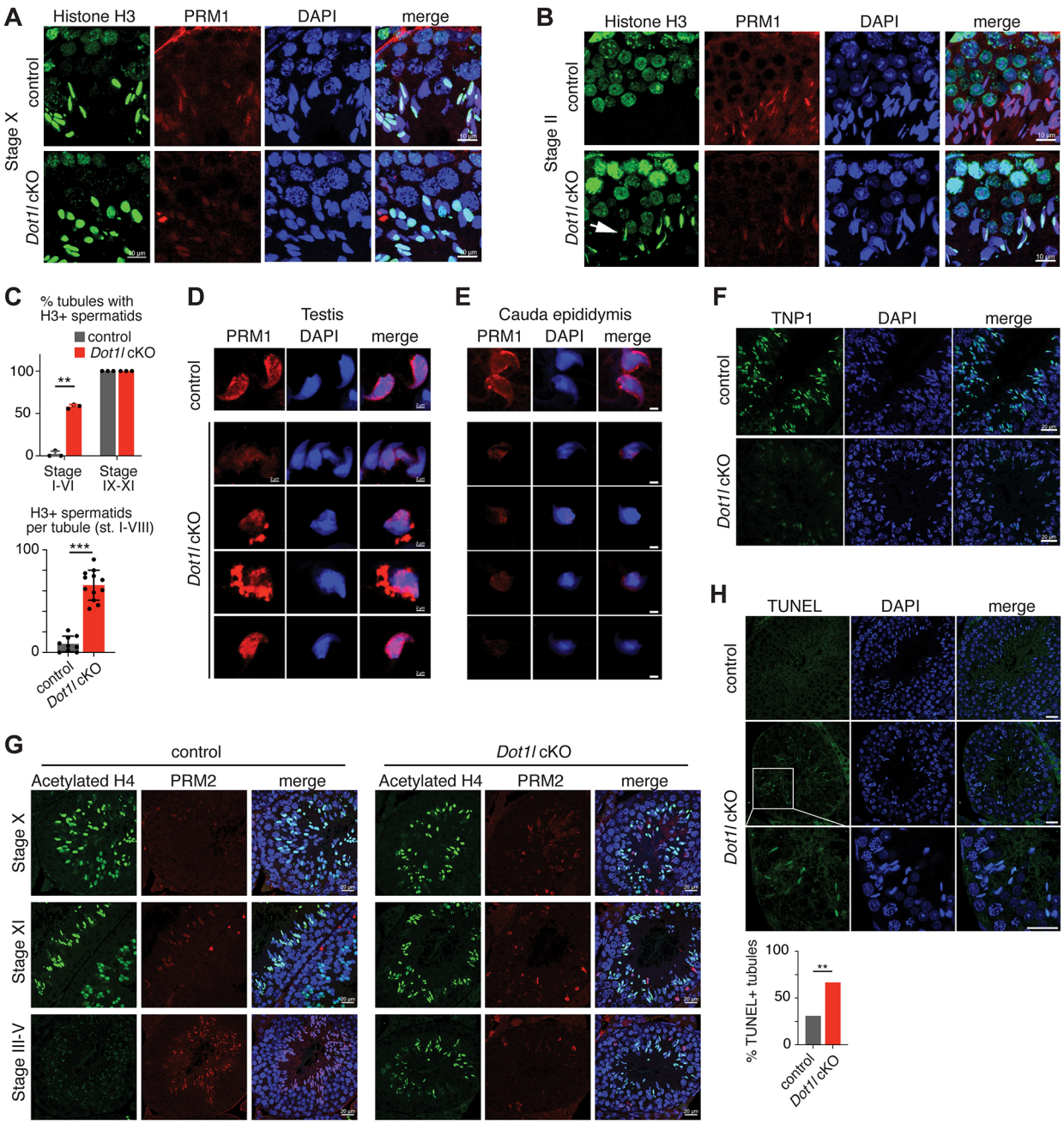

Fig. 5. DOT1L regulates key events in the histone-to-protamine transition in elongating spermatids. (A,B) Immunofluorescence staining for histone H3 and PRM1 in control (*Dot1l*$^{fl/+}$; *Cre*−) and *Dot1l* cKO (*Dot1l*$^{fl/\Delta}$; *Cre*+) stage X (A) and stage II (B) tubules. Arrow in B indicates spermatids with retained histones. DNA was counterstained with DAPI. Scale bars: 10 µm. (C) Top: quantitation of spermatid histone retention in tubule stages I-VI, when spermatids do not normally retain histones, and stages IX-XI, when spermatids have not yet undergone histone-to-protamine replacement. Data represent at least nine tubules in each stage group from *n*=3 animals. ***P*<0.01 (two-tailed paired *t*-test). Bottom: percentage of total elongated spermatids per tubule that are H3^{+}. Analysis was restricted to tubule stages I-VIII, when elongated spermatids normally do not stain for H3. Data are mean±s.d. for 30-120 spermatids in *n*=9 (control) or *n*=12 (*Dot1l*) tubules from two mice of each genotype. ****P*<0.0001 (two-tailed unpaired *t*-test with Welch's correction). (D) Immunofluorescence for PRM1 in elongated spermatid squash preparations in control and *Dot1l* cKO mice. DNA was counterstained with DAPI. Scale bars: 2 µm. (E) Immunofluorescence for PRM1 in squash preparations of germ cells isolated from the cauda epididymis of control and *Dot1l* cKO mice. DNA was counterstained with DAPI. Scale bars: 2 µm. (F) Immunofluorescence for transition protein 1 (TNP1, green) in elongated spermatids in testis cross-sections from control and *Dot1l* cKO mice. DNA was counterstained with DAPI. Scale bars: 20 µm. (G) Immunofluorescence for acetylH4 and PRM2 in testis cross-sections of control and *Dot1l* cKO mice at the indicated tubule stages. DNA was counterstained with DAPI. Scale bars: 20 µm. (H) TUNEL staining in stage IV-V elongating spermatids of control and *Dot1l* cKO testis cross-sections. Bottom row shows areas outlined in the row above at higher magnification. DNA was counterstained with DAPI. Scale bars: 20 µm. Graph shows quantitation of tubules containing TUNEL^{+} cells. There are at least 10 tubules in each category from *n*=2 animals. ***P*<0.01 (Fisher's exact test).

was the most terminal population of elongating spermatids (ES-3), which were substantially reduced in number in the *Dot1l* cKO, consistent with a model where DOT1L is required for spermiogenesis (Fig. 6B). We assessed differential gene expression between control and *Dot1l* cKO cell populations within each cluster, accounting for the reduced numbers of

Development (2023) 150, dev201497. doi:10.1242/dev.201497

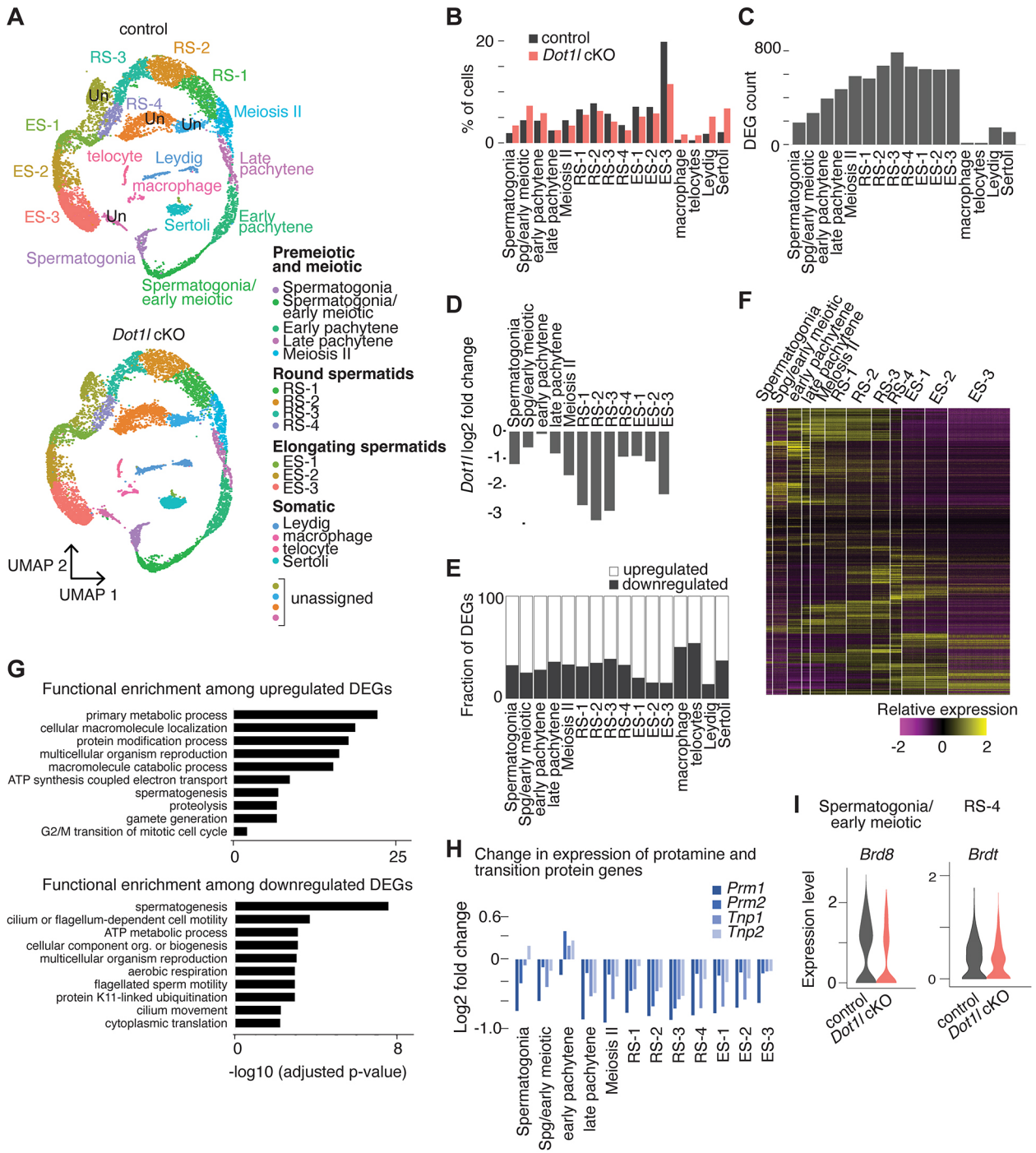

Fig. 6. Loss of DOT1L perturbs the postmeiotic transcriptional program. (A) UMAP plot of single cell RNA-seq (scRNA-seq) datasets from control (*Dot1l*$^{fl/+}$; *Cre*−) and *Dot1l* cKO (*Dot1l*$^{fl/\Delta}$; *Cre*+) showing post-harmonization spermatogenic clusters. (B) Fraction of cells falling in each cluster for control and *Dot1l* cKO datasets. (C) Number of differentially expressed genes (DEGs) in each cluster. (D) Change in levels of *Dot1l* transcript in *Dot1l* cKO compared with control in each spermatogenic cell cluster. (E) Fraction of DEGs that are up- or downregulated in each cluster. (F) Heatmap showing expression levels for each DEG in wild-type cells across spermatogenesis. (G) Gene ontology enrichments among up- and downregulated DEGs across all clusters. (H) Relative expression of protamine and transition protein transcripts in *Dot1l* cKO compared with control in each spermatogenic cell cluster. (I) Violin plots showing distribution of transcript levels for *Brd8* in spermatogonia/early meiotic cells and *Brdt* in late round spermatids (cluster RS-4).

elongating spermatids in the *Dot1l* cKO. We defined a large number of gene expression changes induced by the loss of DOT1L: a total of 2204 unique genes were misregulated in the *Dot1l* cKO across all clusters, with the highest number of differentially expressed genes (DEGs) occurring in postmeiotic stages (Fig. 6C, Table S2). To address the possibility that the apparent differences in gene expression were secondary to differences in cluster assignments between control and *Dot1l* cKO datasets, we assessed the probabilities that cluster assignments in the *Dot1l* cKO matched those defined in the control dataset and confirmed that clusters were equivalently assigned between the datasets (Fig. S3A). Expression of *Dot1l* itself was significantly downregulated across multiple

Development (2023) 150, dev201497. doi:10.1242/dev.201497

clusters, further validating the knockout (Fig. 6D, Fig. S3B). Contrary to expectations based on the known role of DOT1L as a transcriptional activator, there was a mild bias toward upregulation among DEGs (Fig. 6E). Upregulation of this set of genes may be an indirect effect of DOT1L loss. We plotted the relative expression of each DEG across spermatogenesis in wild-type cells and found that while DEG expression patterns varied, a large fraction were most highly expressed at postmeiotic stages (Fig. 6F). Functional enrichment analysis of the sets of upregulated or downregulated genes across all stages revealed enrichment for spermatogenesis functions among genes of both classes, as well as metabolic processes and cell cycle regulation among upregulated genes, and sperm motility and aerobic respiration among downregulated genes (Fig. 6G). Finally, we examined the specific genes that were most strongly downregulated in *Dot1l* cKO cells. These encompassed multiple genes required for spermiogenesis, including *Tnp1*, *Tnp2*, *Prm1* and *Prm2* (Fig. 6H), but not *H2al2a*, which encodes the histone variant H2A.L.2 (Fig. S3C). We also observed a more modest downregulation of *Brdt* in late round spermatids and the bromodomain homolog *Brd8* in early meiotic cells (Fig. 6I). Unexpectedly, we also found misregulation of transcripts corresponding to epigenetic repressors, suggesting that some of the effects of DOT1L on chromatin regulation may be indirect and mediated by misexpression of other chromatin regulators, such as *Erh*, *Kdm5b* and *Suv39h2* (Fig. S3D). Together, these results indicate that although loss of DOT1L does not significantly influence the distribution of spermatogenic cell populations, it causes substantial transcriptional misregulation of genes involved in nuclear condensation during spermiogenesis, with the strongest effect concentrated in postmeiotic cells.

DOT1L deposits H3K79me2 at *Brdt* and contributes to spermatid chromocenter stability

The results of our scRNA-seq analysis indicate that although all spermatogenic cell types are present in *Dot1l* cKO testes, there are significant changes in gene expression within each cell type. Although many of these changes are likely to be indirect effects, the extensive transcriptional defects and known molecular function of DOT1L as a transcriptional activator strongly suggest that DOT1L directly regulates the spermatogenic transcriptome. We selected some known markers of spermatogenesis that are required at meiotic or postmeiotic spermatid differentiation stages (*Sycp3*, *Tnp1*, *Tnp2*, *Prm1*, *Prm2*, *Brdt*, *Brd2* and *Brd4*) and validated the observed changes in expression by RT-qPCR. Consistent with the scRNA-seq data, this analysis showed significantly reduced levels for the protamine and transition protein genes *Prm1*, *Prm2* and *Tnp1* (Fig. 7A), and a trend toward downregulation for the other markers. The stronger effect on transition protein and protamine genes is consistent with the scRNA-seq data and supports a specific role for DOT1L in regulating postmeiotic chromatin remodeling and sperm head condensation. We also tested the protein levels of PRM2 and BRDT, both of which are essential for sperm-specific chromatin compaction, by western blotting and found that levels of both proteins were reduced in *Dot1l* cKO testis compared with control (Fig. 7B).

The finding that BRDT is reduced in the absence of DOT1L is intriguing because BRDT is a sperm-specific histone reader that binds to acetylH4, has bromodomain-dependent functions in post-meiotic spermatid development and is required for appropriate spermatid condensation (Gaucher et al., 2012). DOT1L may therefore regulate spermiogenesis partly through direct regulation of transition protein and protamine genes, and partly through indirect regulation of these genes via regulation of *Brdt*. To more deeply understand how DOT1L regulates *Brdt* expression during spermiogenesis, we performed chromatin immunoprecipitation followed by qPCR (ChIP-qPCR) for the DOT1L-dependent histone modification H3K79me2 in control and *Dot1l* cKO round spermatids isolated by flow cytometry. H3K79me2 was strongly enriched at the *Brdt* locus in control spermatids and this enrichment was dependent on DOT1L (Fig. 7C). We then performed ChIP-qPCR for elongating RNA Pol II (phosphorylated at serine 2, RNA Pol II S2-P) in flow-sorted round spermatids. DOT1L interacts with RNA Pol II at transcriptional start sites to mediate gene transcription (Kim et al., 2012; Steger et al., 2008), and we reasoned that DOT1L could regulate *Brdt* expression by recruiting RNA Pol II and/or promoting transcriptional elongation. We found that Pol II S2-P enrichment at the *Brdt* promoter was also DOT1L dependent, as a 50% reduction in RNA Pol II S2-P at *Brdt* was observed in *Dot1l* cKO compared with the control spermatids (Fig. 7D). These data implicate DOT1L as a direct transcriptional regulator of *Brdt*, a gene that is crucial for sperm-specific chromatin remodeling.

In addition to its role as a transcriptional activator at single-copy genes, DOT1L has also been shown to promote major satellite transcription in mouse embryonic stem cells (Malla et al., 2021 preprint). Major satellite transcripts increase in abundance in condensing spermatids and have been suggested to be important for the histone-to-protamine transition (Hoghoughi et al., 2020). Major satellite transcription is required for structural integrity of chromocenters, which are DAPI-dense heterochromatic regions composed mostly of major satellite repeats that are thought to facilitate compaction of the genome in elongating spermatids (Saksouk et al., 2015; Probst et al., 2010; Velazquez Camacho et al., 2017; Meyer-Ficca et al., 1998; Haaf and Ward, 1995; Prakash Yadav et al., 2023; Yadav et al., 2020). Therefore, we considered the possibility that, in addition to regulating expression of genes important for the histone-to-protamine transition, DOT1L also promotes this transition by enhancing expression of major satellite transcripts. We evaluated transcript levels corresponding to the mouse major satellite sequence and found a substantial decrease in major satellite transcripts in *Dot1l* cKO testis (Fig. 7E). Correspondingly, we observed a significant disruption of chromocenter morphology in round spermatids of *Dot1l* cKO mice (Fig. 7F,G). Changes in major satellite expression and chromocenter integrity may combine with reduced production of transition proteins and protamines to contribute to defective chromatin condensation in *Dot1l* cKO spermatids. Interestingly, BRDT has itself been implicated in regulation of chromocenter formation in testis, although this effect was variable and dependent on genetic background (Berkovits and Wolgemuth, 2011). DOT1L could thus regulate chromocenter structure both through direct regulation of major satellite transcription and indirectly through regulation of BRDT levels. Together, these results establish DOT1L as an essential chromatin regulator that drives transcriptional programs needed to bring about the complex nuclear remodeling required for sperm formation and function.

DISCUSSION

Here, we demonstrate that the histone modifier DOT1L is essential for histone removal and sperm head condensation during spermiogenesis, and that its loss in spermatids leads to defective chromatin remodeling, which ultimately results in abnormal sperm head morphogenesis and infertility. We find that enrichment of DOT1L-dependent H3K79 methylation coincides with the timing of spermatid elongation and condensation during spermatogenesis,

Development (2023) 150, dev201497. doi:10.1242/dev.201497

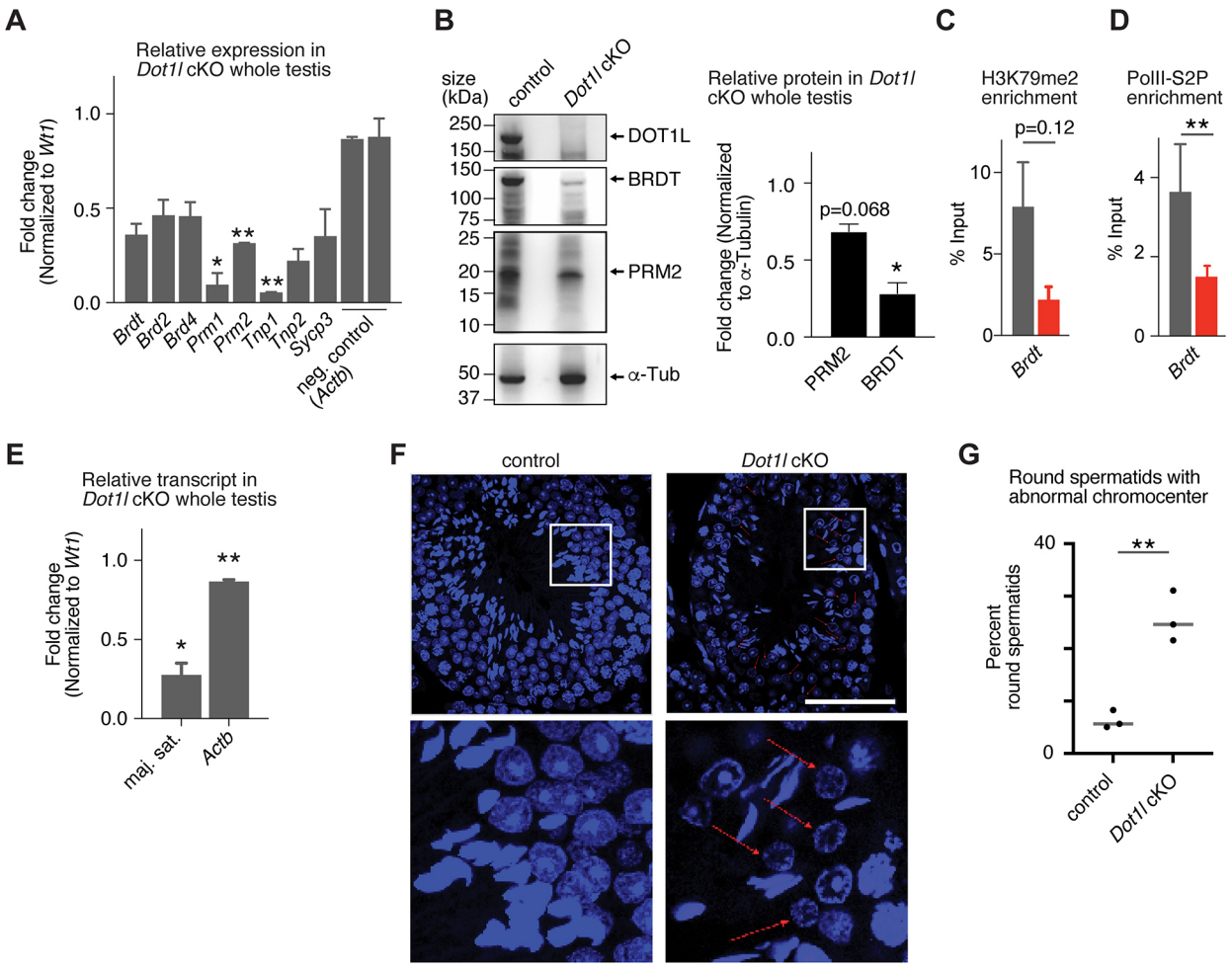

Fig. 7. DOT1L activates transcription of genes required for the histone-to-protamine transition. (A) RT-qPCR of selected spermatogenesis genes in whole testis of control (*Dot1l*$^{fl/+}$; *Cre*−) and *Dot1l* cKO (*Dot1l*$^{fl/\Delta}$; *Cre*+) adult animals. Data are the mean fold change in *Dot1l* cKO compared with control. Wilms tumor 1 (*Wt1*) was used as an internal control. Data are mean±s.e.m. $^{**}P<0.001$, $^{*}P<0.05$ (two-tailed unpaired *t*-test). (B) Western blot for DOT1L, BRDT and PRM2 in adult control and *Dot1l* cKO testis. α-Tubulin is a loading control. Right, quantification of fold change in band intensity for *Dot1l* cKO relative to control after normalizing to α-tubulin. $n=2$ biological replicates. $^{*}P<0.05$ (two-tailed unpaired Welch's *t*-test). (C) ChIP-qPCR for H3K79me2 at the *Brdt* promoter in control and *Dot1l* cKO round spermatids isolated by flow cytometry. Percent input values were normalized within each genotype to a negative control intergenic locus (mm10 chr19:51758385-58758494) that is not expected to be enriched for H3K79me2. Data are mean±s.e.m. for $n=3$ biological replicates. $P=0.12$ (two-tailed unpaired *t*-test). (D) ChIP-qPCR for RNA Pol II S2P at the *Brdt* promoter in control and *Dot1l* cKO round spermatids isolated by flow cytometry. Values were normalized as in C. Data are mean±s.e.m. for $n=3$ biological replicates. $^{**}P<0.01$ (two-tailed unpaired *t*-test). (E) RT-qPCR for major satellite transcripts in whole testis tissue of control and *Dot1l* cKO adult animals. Data are mean±s.e.m. fold change in *Dot1l* cKO compared with control for $n=2$ biological replicates. Wilms tumor 1 (*Wt1*) was used an internal control. $^{**}P<0.001$, $^{*}P<0.05$ (two-tailed unpaired *t*-test). (F) DAPI-stained cross-sections of adult control and *Dot1l* cKO testis. Red arrows indicate disrupted chromocenters in round spermatids. Scale bar: 20 µm (upper panels); 5 µm (lower panels). (G) Quantification of round spermatids with disrupted chromocenters. Horizontal lines represent the mean of $n=3$ biological replicates representing a total of $n=390$ (control) or $n=230$ (*Dot1l* cKO) round spermatids. $^{**}P<0.001$ (two-tailed unpaired *t*-test).

and show that DOT1L serves as an important driver of transcriptional programs that are required for postmeiotic maturation of round spermatids to elongated spermatids. We find that DOT1L deposits H3K79me2 at *Brdt* and may help to promote transcriptional elongation by RNA Pol II, ultimately enhancing expression at this locus and other genes that are essential for sperm DNA condensation. Furthermore, we show that abnormal elongating spermatids in *Dot1l* cKO testes are likely eliminated by apoptosis. Our data suggest that the male sterility phenotype observed in *Dot1l* germline conditional knockouts is due in part to defects in postmeiotic spermatid differentiation in addition to the loss of premeiotic spermatogonial stem cells that has been reported previously (Lin et al., 2022). Our findings are consistent with those of Lin et al. (2023) showing a requirement for DOT1L beyond the spermatogonial stem cell stage, aberrant retention of histones in epididymal sperm of *Dot1l* cKO males, and co-dependence between DOT1L and the transcriptional elongation co-factor MLLT10 (AF10) during spermatogenesis.

We found that the expression of DOT1L peaks during meiotic to postmeiotic transition and that a large fraction of transcriptional changes in expression occur after meiosis (Fig. 6C), supporting the involvement of DOT1L in postmeiotic germ cell development and spermatid differentiation. Specifically, we found that genes required for normal spermatid elongation and chromatin condensation, including *Tnp1*, *Tnp2*, *Prm1* and *Prm2* (Cho et al., 2001; Shirley et al., 2004) are significantly downregulated in *Dot1l* cKO spermatids (Figs 6H and 7A). We also detected a robust downregulation of *Brdt* transcript by qPCR and downregulation of BRDT protein by western blot, as well as a trend toward downregulation in spermatids in our scRNA-seq dataset. DOT1L is known to interact with the C-terminal

Development (2023) 150, dev201497. doi:10.1242/dev.201497

domain of RNA Pol II and to recruit it to active chromatin (Mohan et al., 2010; Kim et al., 2012). Together with altered deposition of H3K79me2 and differential enrichment of elongating RNA Pol II at spermiogenic loci, our findings suggest that a requirement for DOT1L-mediated transcriptional activation of spermiogenesis genes explains the defects in sperm head packaging and chromatin condensation observed in the *Dot1l* cKO. DOT1L could be acting via the DotCom complex to promote sperm-specific transcriptional activation, as has been reported for somatic cells (Mohan et al., 2010), consistent with the genetic and physical interaction with MLLT10 in testes reported by Lin et al. (2023), and possibly with participation of some unknown spermatogenesis-specific complex components.

The central finding of this study is that DOT1L loss causes defective histone removal that results in abnormal chromatin condensation in elongating spermatids, as well as partial disruption of chromocenter formation in round spermatids. Several consequences of DOT1L loss could mediate these effects. First, expression of protamines and transition proteins, which are essential for normal histone removal and chromatin condensation, were reduced in *Dot1l* cKO spermatids (Merges et al., 2022; Cho et al., 2001; Zhao et al., 2004a,b). Second, we find that loss of DOT1L impairs transcription of the gene encoding BRDT (Figs 6I, 7B-D), a testis-specific bromodomain protein known to bind acetylated H4 and facilitate histone eviction during spermiogenesis (Morinière et al., 2009; Gaucher et al., 2012; Goudarzi et al., 2016; Shiota et al., 2018), implying that reduced BRDT expression may mediate some of the phenotypes observed in *Dot1l* cKO spermatids. Finally, reduced expression of major satellite repeat transcripts in *Dot1l* cKO spermatids may contribute to chromocenter destabilization and associated protamine replacement defects. Major satellite transcription has been shown to stabilize chromocenter structures in spermatids and other cell types, facilitating histone-to-protamine replacement; our group recently reported that DOT1L selectively promotes major satellite expression to stabilize heterochromatin in mouse embryonic stem cells (Malla et al., 2021preprint; Saksouk et al., 2015; Probst et al., 2010; Velazquez Camacho et al., 2017; Meyer-Ficca et al., 1998; Haaf and Ward, 1995; Yadav et al., 2020; Prakash Yadav et al., 2023). Interestingly, spermatids homozygous for mutant BRDT lacking the first bromodomain ($Brdt^{\Delta BD1/\Delta BD1}$) also exhibit chromocenter disruption, although this effect is variable and dependent on genetic background (Berkovits and Wolgemuth, 2011), implying that DOT1L may regulate chromocenter stability at multiple levels.

Our scRNA-seq data reveal that there are few substantial differences in the populations of germ cells present in the testis of the *Dot1l* cKO, a result supported by our flow cytometry data, although scRNA-seq analysis did confirm the reduction in elongating spermatids detected in our histological and immunofluorescence data (Figs 3 and 6). We note that it is possible that changes in cell differentiation induced by loss of DOT1L could affect cell type assignment in the scRNA-seq data and bias cell type-specific differential gene expression calls, although our analysis confirms high confidence in cluster assignments across genotypes. DOT1L was recently shown to be required for maintenance of spermatogonial stem cells (SSCs) (Lin et al., 2022). Using the same conditional knockout model, we observed that the SSC defect appeared incompletely penetrant, with about 25% of seminiferous tubules exhibiting complete loss of germ cells (Sertoli cell only phenotype) at 3-6 months of age (Fig. 3). This result suggests that loss of DOT1L does not affect all SSCs equally. Current models support the co-existence of multiple subpopulations of neonatal spermatogonia defined by different cell surface markers, where SSCs expressing high levels of *Id4* constitute a true stem cell population and are a subset of undifferentiated spermatogonia identified by PLZF/ZBTB16 and CDH1, while a separate pool of initial differentiating spermatogonia expresses STRA8 and cKIT (Niedenberger et al., 2015; Law and Oatley, 2020). It is possible that loss of DOT1L specifically depletes only some of these populations, resulting in the incompletely penetrant spermatogonial phenotype we observed. Our scRNA-seq analysis did not reveal loss of a specific spermatogonial population in *Dot1l* cKO testis, but the small size of spermatogonial subpopulations may have precluded their detection in our whole-testis dataset. We confirmed complete loss of male fertility upon DOT1L deletion, in agreement with the previous report (Lin et al., 2022). The presence of abundant meiotic and postmeiotic cells in our sterile adult *Dot1l* cKO males indicates that postmeiotic defects also contribute substantially to the sterility phenotype.

In summary, our results establish DOT1L as an essential regulator of sperm-specific gene transcription and highlight its importance in histone removal and chromatin condensation during spermatid differentiation. Together, our data reveal that a major reason for male sterility observed upon loss of DOT1L is defective histone-to-protamine replacement in elongating spermatids. Interestingly, H3K79me2 is one of a handful of histone modifications reported to be retained at a higher frequency in defective compared with normal human sperm (La Spina et al., 2014). Along with the previously reported spermatogonial defect, our findings emphasize that DOT1L has multiple crucial functions during spermatogenesis. Our results advance mechanistic understanding of sperm morphogenesis and suggest new directions for future studies of infertility and contraception.

MATERIALS AND METHODS

Mouse breeding and maintenance

These studies were approved by the Yale University Institutional Animal Care and Use Committee under protocol 2020-20169. All mice (*Mus musculus*) were maintained and euthanized according to the principles and procedures described in the National Institutes of Health guide for the care and use of laboratory animals. All mice were on a C57BL/6J genetic background. *Dot1l* cKO male mice were generated by crossing $Dot1l^{flox/flox}$ (Bernt et al., 2011) females with male mice harboring one copy of *Ddx4-Cre* transgene ($B6\text{-}Ddx^{4tm1.1(cre/mOrange)Dcp}$), which is first expressed in germ cells at embryonic day 15.5 (Gallardo et al., 2007; Hu et al., 2013). Mouse genotyping was performed as defined previously (Bernt et al., 2011). Males between 2 and 5 months of age were used except where otherwise specified. Primers used for genotyping are listed in Table S3.

Histology

Testes and epididymides were dissected from control and *Dot1l* cKO male mice at matched ages. After isolation, tissues were briefly washed with phosphate-buffered saline (PBS) and fixed in Hartman's fixative (Millipore-Sigma; H0290-500ML) for 48 h at room temperature. To remove the last traces of fixative, samples were washed in 70% ethanol, dehydrated and embedded in paraffin wax. Sections (4 µm) were prepared on glass slides, cleared in xylene and dehydrated in a graded series of ethanol. The sections were then stained with Hematoxylin and Eosin. Images were acquired with a bright-field light microscope (Zeiss Axio Lab A1 Bright Field Microscope, 20×0.5 NA or 40×0.75 NA objectives). Stages of the seminiferous epithelia were identified according to established methods (Russell et al., 1990; Ahmed and de Rooij, 2009).

Immunofluorescence staining

Paraffin wax-embedded testis sections were deparaffinized in xylene, dehydrated in a graded series of ethanol, boiled in 10 mM sodium citrate buffer (pH 6) in a microwave oven for 20 min to retrieve the antigen, washed

Development (2023) 150, dev201497. doi:10.1242/dev.201497

in PBS, permeabilized in 0.5% Triton X-100 for 10 min, blocked in blocking buffer (5% BSA+0.1% Triton X-100) for 1 h at room temperature and then incubated overnight at 4°C with primary antibodies (Table S4) diluted in blocking buffer. The slides were washed with PBS and stained with fluorophore-conjugated secondary antibodies, including AlexaFluor 488-conjugated or AlexaFluor 568-conjugated goat anti-rabbit-IgG (Molecular Probes) and AlexaFluor 568-conjugated goat anti-mouse-IgG (Molecular Probes). See Table S4 for a complete listing of antibodies and dilutions. All secondary antibodies were used at 1:500 dilution in blocking buffer and incubated at room temperature for 1 h. Finally, slides were mounted in antifade mounting medium containing DAPI (H-1200, Vector Labs). Images were acquired with an LSM 880 (LSM acquisition software) or LSM 980 airyscan confocal microscope (Zeiss) equipped with 405, 488 or 555/561 nm lasers, and fitted with a 63×1.4 NA objective. Images were processed with Zen acquisition software.

TUNEL staining

TUNEL staining was performed using an APO-BrdU TUNEL assay kit (Sigma-Aldrich, A35125) according to the manufacturer's instructions. Briefly, testis sections were deparaffinized as stated above and then labelled with BrdU in the presence of terminal deoxynucleotidyl transferase (TdT) enzyme for 2 h at 37°C. After two washes, the sections were incubated with AlexaFluor 488-conjugated anti-BrdU antibody supplied with the kit for 1 h at room temperature. The slides were mounted antifade mounting medium containing DAPI and imaged as described above.

Immunoblotting

Testes from control and *Dot1l* cKO male mice were dissected and briefly washed in chilled 1× PBS. Tunica albuginea were removed, and seminiferous tubules were minced and collected in RIPA buffer [50 mM Tris-HCl (pH 7.4), 150 mM NaCl, 1% Triton X-100, 0.5% sodium deoxycholate, 0.1% SDS, 1 mM EDTA, 10 mM NaF and 1 mM PMSF] containing freshly prepared cOmplete EDTA-free protease inhibitor cocktail (Roche, 11873580001). Tissues were subjected to homogenization and sonication in a Bioruptor Pico (Diagenode). Cell extracts were centrifuged at 20,000× ***g*** for 15 min at 4°C and supernatants were immediately mixed with 4× SDS sample buffer to a final dilution of 1×. The samples were heated at 95°C for 5 min, resolved on a Mini-PROTEAN TGX gel (Bio-Rad, 456-8093) by SDS-PAGE for 2 h at 80 V and transferred onto PVDF membranes (GE Healthcare) in 20 mM Tris-HCl (pH 8.0), 150 mM glycine and 20% methanol. After transfer, membranes were blocked with 5% skimmed (non-fat) milk for 1 h at room temperature, followed by incubation with the primary antibody overnight at 4°C. After washing three times with TBST buffer [20 mM Tris-HCl (pH 7.6), 150 mM NaCl and 0.1% Tween 20), membranes were incubated at room temperature for 1 h with HRP-conjugated secondary antibodies as follows: goat anti-rabbit IgG conjugated to HRP (Jackson ImmunoResearch, 111-035-003, 1:20,000) for DOT1L and BRDT, and goat anti-mouse IgG conjugated to HRP (Jackson ImmunoResearch, 111-035-003, 1:20,000) for PRM2 and alpha-tubulin. See Table S4 for a complete list of antibodies and dilutions. After washing the membrane three times with TBST, specific protein bands were detected using a SuperSignal West Pico PLUS Chemiluminescent Substrate (Thermo Fisher Scientific, 34577). Chemiluminescence was detected using the FluorChem E (Protein Simple) documentation system. Densitometry analysis of bands was performed by using ImageJ (Fiji) software. The band intensity of the protein of interest was normalized to the loading control.

Preparation of testicular cell suspensions

Flow cytometry

Testes from 25 day post partum (dpp) mice were dissected, the tunica albuginea was removed and the seminiferous tubules were minced in Ca^{2+}- and Mg^{2+}-free PBS (Gibco). Cells were dispersed by gentle aspiration, filtered using a 40 µm nylon filter, and washed in PBS by centrifuging at 800× ***g*** for 5 min. The cells were re-suspended in PBS, fixed in 70% chilled ethanol, and stored at 4°C for 24 h or at −20°C for up to 1 week until further analysis. 1×10^6-2×10^6 ethanol-fixed testicular cells were washed with PBS and treated with 0.25% pepsin solution for 10 min at 37°C. Finally, cells were stained with propidium iodide (PI) staining solution (25 µg/ml PI, 40 mg/ml RNase and 0.03% Nonidet P-40 in PBS) at room temperature for 20 min. The PI-stained cells were analyzed on an Bio-Rad S3e cell sorter (Bio-Rad; excitation 488 nm; emission 585/40 nm).

Single cell RNA-seq

Decapsulated testes were incubated in DMEM containing 0.75 mg/ml collagenase type IV (Gibco, 17104-019) for 10 min at 37°C with occasional inversion. An equal volume of DMEM was added to the suspension of dissociated tubules before centrifuging at 400 ***g*** for 5 min at 4°C. After removing the supernatant, the cell pellet was washed in DMEM and resuspended in 0.05% trypsin-EDTA (Gibco, 25200-056) for 10 min incubation at room temperature. An equal volume of ice-cold DMEM+10% FBS was then added to the cell suspension before washing the pellet twice with media. The cell pellet was resuspended in DPBS (Sigma-Aldrich, D8537) containing 0.04% bovine serum albumin (Sigma-Aldrich, A9647) and filtered through a 100 µm filter (Falcon, 22363549) then a 40 µm filter (Falcon, 352340) to generate a single cell suspension.

All other applications

Testicular cell suspensions were prepared as previously reported (Yeh et al., 2021). Decapsulated testes were briefly washed with ice-cold Dulbecco's phosphate-buffered saline (DPBS, Gibco). Seminiferous tubules were gently dispersed and untangled with forceps and transferred to fresh petri dish. This was repeated three times to remove interstitial cells as much as possible. Untangled seminiferous tubules were incubated in DMEM containing 1.5 mg/ml hyaluronidase (Millipore Sigma, H3506), 0.25 mg/ml DNase I (Stem Cell Technologies, 07900), collagenase type IV (2 mg/ml) and FBS (2%) in a 15 ml tube at 37°C for 20 min. Tubules were gently pipetted until no visible chunks remained. An equal volume of ice-cold DMEM+10%FBS was then added to the cell suspension. Cells were centrifuged at 300 ***g*** for 5 min at room temperature and supernatant was discarded. The pellet was resuspended in 10 ml of FACS buffer (DPBS with 2% FBS) and cells were filtered through a 40 µm filter (Falcon, 352340) to generate a single cell suspension.

Chromatin immunoprecipitation-qPCR in sorted round spermatids

Testicular cells in suspension were crosslinked with 1% formaldehyde at room temperature for 10 min. Formaldehyde was quenched with 0.1375 M glycine at room temperature for 10 min. Fixed cells were spun down at 300 ***g*** for 5 min at 4°C. The pellet was washed twice with FACS buffer. Total testicular cells were stained with PI staining solution as described above and round spermatids (1C cell population) were isolated using a Bio-Rad S3e cell sorter. 1×10^6 round spermatids were washed with ice-cold DPBS and pelleted. The pellet was resuspended in 50 µl chromatin immunoprecipitation (ChIP) lysis buffer (1% SDS, 10 mM EDTA and 50 mM Tri-HCl at pH 8.1) and frozen at −80°C. To prepare antibody-bound Dynabeads (Thermo Fisher Scientific, 10007D), 10 µl Dynabeads were washed twice with 150 µl of block solution (0.5% BSA in PBS) and resuspended in 30 µl block solution. 1 µg antibody per million cells was added to each aliquot of beads and incubated for 8 h rotating at 4°C. Frozen cells were thawed on ice and ChIP dilution buffer (0.01% SDS, 1.1% Triton X-100, 1.2 mM EDTA, 167 mM NaCl and 16.7 mM Tris-HCl at pH 8.1) was added to reach a total volume of 150 µl. Cells were sonicated at 4°C for 20 cycles (30 s on/off) using a Bioruptor bath sonicator (Diagenode). Aliquots of the same samples were pooled and spun down at 12,000 ***g*** for 5 min. The supernatant was moved to a new 1.5 ml Eppendorf tube and brought up to 1 ml with 750 µl ChIP dilution buffer and 100 µl protease inhibitor cocktail (Roche, 11836153001). 50 µl of each sample was set aside as input, and then an aliquot of antibody-bound Dynabeads was added to the lysate and incubated overnight at 4°C with rotation. After overnight incubation, beads were washed twice with low-salt immune complex wash buffer (0.1% SDS, 1% Triton X-100, 2 mM EDTA, 150 mM NaCl and 20 mM Tris-HCL at pH 8.1), twice with LiCl wash buffer (0.25 M LiCl, 1% NP40, 1% deoxycholate, 1 mM EDTA and 10 mM Tris-HCl at pH 8.1) and twice with TE (1 mM EDTA and 10 mM Tris-HCl at pH 8.0). Bound DNA

Development (2023) 150, dev201497. doi:10.1242/dev.201497

was eluted twice with 125 µl elution buffer (0.2% SDS, 0.1 M NaHCO3 and 5 mM DTT in TE) at 65°C and crosslink reversal was performed by incubating at 65°C for 8-15 h. ChIP and input samples were incubated for 3 h at 37°C with 0.2 mg/ml RNAse A (Millipore, 70856-3) and for 4-10 h at 55°C with 0.1 mg/ml Proteinase K (NEB P8107S). Sample DNA was isolated using a Zymo ChIP DNA Clean & Concentrator kit (Zymo Research, D5201) according to the manufacturer's instructions. DNA was eluted with 20 µl Elution Buffer into fresh Eppendorf tubes, then re-eluted with the same eluate to enhance the yield.

RNA isolation and reverse transcription

Testes from control and *Dot1l* cKO male mice were dissected and briefly washed in chilled 1× PBS. After removing tunica albuginea, seminiferous tubules were minced and thoroughly homogenized in 1 ml of TRIzol reagent (Invitrogen, 15596026). After 5 min of incubation, the lysate was mixed with 200 µl of chloroform and centrifuged at 12,000 ***g*** for 15 min at 4°C. The aqueous phase was mixed with an equal volume of 100% ethanol and transferred to an RNeasy MinElute spin column (Qiagen, 74104) for purification of total RNA according to the manufacturer's instructions. Reverse transcription of 1 µg of total RNA was performed with random hexamer primers and iScript reverse transcriptase (Bio-Rad, 1708896) in a total volume of 20 µl according to the manufacturer's instructions. Reaction mixtures were incubated in a thermocycler at 25°C for 5 min then 42°C for 60 min before stopping the reaction at 85°C for 5 min.

Real-time quantitative PCR

For ChIP-qPCR, 1 µl each of eluted ChIP and input DNA was used for qPCR in 20 µl reaction containing 1 µM forward/reverse primer mix, 1× Power SYBR Green PCR Master Mix (Applied Biosystems, 4367659) and 5.6 µl nuclease-free water. Reactions for each target gene were performed in duplicate in a 96-well plate loaded into an Applied Biosystems QuantStudio 3 Real-Time PCR system under standard cycling conditions.

For reverse transcription qPCR (RT-qPCR), 1 µl of undiluted cDNA was used for a 20 µl reaction volume consisting of 4 µl of 10 µM forward plus reverse primer mix, 10 µl of Power SYBR Green PCR Master Mix (Applied Biosystems, 4367659) and 5 µl nuclease-free water. Relative fold change in transcript abundance was calculated using the delta-delta Ct method by normalizing target gene expression levels to either *Actb* or *Wt1*.

Reactions for each target gene were performed in duplicate in a 96-well plate loaded into an Applied Biosystems QuantStudio 3 Real-Time PCR System. Standard cycling conditions were used: for hold stage (×1), 50°C for 2 min, 95°C for 10 min; for PCR stage (×40), 95°C for 15 s, 60°C for 1 min. Melt curve stage conditions were: 95°C for 15 s, 60°C for 1 min and 95°C for 15 s. Primer sequences used for qPCR are listed in Table S3.

Isolation of elongated spermatids from seminiferous tubules

Isolation of elongated spermatids was performed as described previously (Kotaja et al., 2004). Briefly, 12-week-old male mice were euthanized, testes were removed and decapsulated, and seminiferous tubules transferred to a Petri dish containing PBS. When viewed under a transilluminating dissection microscope, seminiferous tubules produce different patterns of light absorption ,giving four different regions: weak spot (stages XII-I), strong spot (stages II-VI), dark zone (stages VII-VIII) and pale zone (stages IX-XI). The dark zone, containing elongated spermatids, was cut into 1 mm long pieces and placed in 50 µl of 100 mM sucrose. Elongated spermatids were obtained in suspension by gentle pipetting of the minced tissue for 1 min. Cells were dried on slides pre-dipped in 1% PFA containing 0.15% Triton X-100. The dried slides were briefly washed in PBS followed by cell fixation in 4% PFA for 10 min and immunofluorescence staining with anti-PRM1 antibody was performed as described above. Slides were mounted in antifade mounting medium containing DAPI (H-1200, Vector Labs). Images were acquired as described earlier.

Preparation of meiotic spermatocyte spreads

Meiotic chromosome spreads were generated as described previously (Peters et al., 1997). Testes were dissected out from mice and collected in DMEM. After removing the tunica albuginea and extracellular material, the seminiferous tubules were briefly washed in cold PBS followed by incubation in hypotonic extraction buffer [30 mM Tris (pH 8.2), 50 mM sucrose, 17 mM trisodium citrate dihydrate, 5 mM EDTA, 0.5 mM dithiothreitol and 0.5 mM phenylmethylsulfonyl fluoride) for 1 h at room temperature. The tubules were then removed from the hypotonic buffer, transferred to a glass slide, and minced with tweezers and scissors to release the cells. 10 µl of cell suspension was diluted with 40 µl 100 mM sucrose and spread onto a glass slide pre-dipped in 1% paraformaldehyde (PFA) containing 0.15% Triton X-100. Slides were dried for 6 h in a humidified chamber before proceeding with immunofluorescence staining. After two washes in PBS, the dried slides were treated with 2% PFA and 0.15% Triton X-100 for 10 min at room temperature and then blocked in blocking buffer (5% BSA+0.1% Triton X-100) for 1 h at room temperature. Slides were then incubated in anti-SYCP3 and H3K79me2/3 antibodies overnight at 4°C. After staining with fluorophore-conjugated secondary antibodies, slides were mounted in antifade mounting medium containing DAPI (H-1200, Vector Labs). Images were acquired using an LSM 980 airyscan confocal microscope (Zeiss, Zen acquisition software) as described above.

scRNA-seq library preparation and analysis

Libraries were prepared with a Chromium Next GEM Single Cell 3′ v3.1 kit (10X Genomics, CG000204) according to the manufacturer's instructions and sequenced on an Illumina NovaSeq machine with 150 base pair paired-end reads. Raw count matrices were generated using CellRanger (10X Genomics). Matrices for the 'WT' and 'KO' samples were imported to R (R Core Team, 2015) using Seurat 4.1.0 (Hao et al., 2021) and combined into one Seurat object. Reads were filtered to exclude cells likely to be doublets or multiplets (nCount_RNA<100,000), dead or dying cells (nFeature_RNA<8000), or cells with high mitochondrial content (percent.mt<mean+standard deviation). This filtered subset was log normalized and scaled. A linear dimensional reduction was performed using principal component analysis (PCA), and 17 dimensions were determined to be appropriate using the 'ElbowPlot()' function. Clusters were identified at a resolution of 0.5, and the 'RunUMAP()' function was used to generate Uniform Manifold Approximation and Projection (UMAP) objects for further analysis. Clusters were associated with stages of spermatogenesis based on expression of key spermatogenic genes. Three of these initial clusters had a low number of detected molecules per cell, indicating dead or dying cells, and did not have any top genes associated with spermatogenesis. Therefore, these three clusters were removed, and the data were normalized, scaled and regressed again using the same parameters described above. The dataset was then integrated using Harmony (Korsunsky et al., 2019), and the 'RunUMAP()', 'FindNeighbors()' and 'FindClusters()' functions were used at a dimensionality of 17 and resolution of 0.5 to generate a final UMAP for further analysis. Cluster identities were again assigned using the same set of key spermatogenic genes applied above. To evaluate the fidelity of cluster assignment between control and *Dot1l* cKO genotypes, cluster identities defined in the control dataset were transferred to the *Dot1l* cKO using the 'TransferData()' function in Seurat and prediction scores were evaluated to confirm a high probability that developmentally equivalent cells were assigned to the same clusters. Differentially expressed genes were determined using the 'FindMarkers()' function. Graphs were produced in R using the ggplot2 package.

Gene ontology (GO) analysis

GO enrichments were evaluated using the GOStats package (Falcon and Gentleman, 2007) in R. *P*-values were adjusted both by conditioning out child categories and by subsequent correction for multiple testing using the Benjamini-Hochberg method.

Statistical methodology

Statistical analyses were performed as indicated in the figure legends. In general, unpaired two-tailed *t*-tests were used for comparison of continuous data, and Welch's correction was applied when the conditions being compared could not be assumed to have the same distribution. Fisher's Exact test was used for categorical data. The threshold for statistical significance was defined as $P<0.05$. No randomization or blinding was performed.

Acknowledgements
We thank Kathrin Bernt for the gift of *Dot1l*^{fl} mice. We appreciate assistance with genotyping from Y. Huang, K. Marshall and C. Kaya, and advice on scRNA-seq analysis from N. Dias. We thank the staff of the Yale Center for Genome Analysis for Illumina sequencing of scRNA-seq data.

Competing interests
The authors declare no competing or financial interests.

Author contributions
Conceptualization: A.B.M., B.J.L.; Validation: A.B.M.; Formal analysis: A.B.M., S.R.R.; Investigation: A.B.M., S.R.R., Z.D.S., B.J.L.; Resources: Z.D.S., B.J.L.; Writing - original draft: A.B.M., S.R.R.; Writing - review & editing: B.J.L.; Visualization: A.B.M., S.R.R., B.J.L.; Supervision: B.J.L.; Funding acquisition: Z.D.S., B.J.L.

Funding
This work was supported by a Rudolph J. Anderson Fellowship to A.B.M., by the National Institutes of Health (DP2HD108774 to Z.D.S., R01HD098128 to B.J.L.), by the G. Harold and Leila Y. Mathers Foundation to Z.D.S., by a Chen Innovation Award to Z.D.S., by the Searle Scholars Program to B.J.L. and by a Pew Scholar Award from the Pew Charitable Trusts to B.J.L. Open Access funding provided by Yale University. Deposited in PMC for immediate release.

Data availability
Single cell RNA-seq data have been deposited in GEO under accession number GSE217931.

Peer review history
The peer review history is available online at https://journals.biologists.com/dev/lookup/doi/10.1242/dev.201497.reviewer-comments.pdf

References

Ahmed, E. A. and de Rooij, D. G. (2009). Staging of mouse seminiferous tubule cross-sections. In *Meiosis: Volume 2, Cytological Methods* (ed. S. Keeney), Methods in Molecular Biology, pp. 263-277. Totowa, NJ: Humana Press, doi:10.1007/978-1-60761-103-5_16 (Accessed November 12, 2022).

Barral, S., Morozumi, Y., Tanaka, H., Montellier, E., Govin, J., de Dieuleveult, M., Charbonnier, G., Couté, Y., Puthier, D., Buchou, T. et al. (2017). Histone variant H2A.L.2 guides transition protein-dependent protamine assembly in male germ cells. *Mol. Cell* **66**, 89-101.e8. doi:10.1016/j.molcel.2017.02.025

Berkovits, B. D. and Wolgemuth, D. J. (2011). The first bromodomain of the testis-specific double bromodomain protein Brdt is required for chromocenter organization that is modulated by genetic background. *Dev. Biol.* **360**, 358-368. doi:10.1016/j.ydbio.2011.10.005

Bernt, K. M., Zhu, N., Sinha, A. U., Vempati, S., Faber, J., Krivtsov, A. V., Feng, Z., Punt, N., Daigle, A., Bullinger, L. et al. (2011). MLL-rearranged leukemia is dependent on aberrant H3K79 methylation by DOT1L. *Cancer Cell* **20**, 66-78. doi:10.1016/j.ccr.2011.06.010

Brewer, L. R., Corzett, M. and Balhorn, R. (1999). Protamine-induced condensation and decondensation of the same DNA molecule. *Science* **286**, 120-123. doi:10.1126/science.286.5437.120

Cho, C., Willis, W. D., Goulding, E. H., Jung-Ha, H., Choi, Y.-C., Hecht, N. B. and Eddy, E. M. (2001). Haploinsufficiency of protamine-1 or -2 causes infertility in mice. *Nat. Genet.* **28**, 82-86. doi:10.1038/ng0501-82

Dhar, S., Thota, A. and Rao, M. R. S. (2012). Insights into role of Bromodomain, Testis-specific (Brdt) in Acetylated Histone H4-dependent chromatin remodeling in mammalian spermiogenesis. *J. Biol. Chem.* **287**, 6387-6405. doi:10.1074/jbc.M111.288167

Dong, Y., Isono, K.-I., Ohbo, K., Endo, T. A., Ohara, O., Maekawa, M., Toyama, Y., Ito, C., Toshimori, K., Helin, K. et al. (2017). EPC1/TIP60-mediated histone acetylation facilitates spermiogenesis in mice. *Mol. Cell. Biol.* **37**, e00017-e00082. doi:10.1128/MCB.00082-17

Dottermusch-Heidel, C., Gärtner, S. M. K., Tegeder, I., Rathke, C., Barckmann, B., Bartkuhn, M., Bhushan, S., Steger, K., Meinhardt, A. and Renkawitz-Pohl, R. (2014). H3K79 methylation: a new conserved mark that accompanies H4 hyperacetylation prior to histone-to-protamine transition in Drosophila and rat. *Biol. Open* **3**, 444-452. doi:10.1242/bio.20147302

Falcon, S. and Gentleman, R. (2007). Using GOstats to test gene lists for GO term association. *Bioinformatics* **23**, 257-258. doi:10.1093/bioinformatics/btl567

Feng, Q., Wang, H., Ng, H. H., Erdjument-Bromage, H., Tempst, P., Struhl, K. and Zhang, Y. (2002). Methylation of H3-lysine 79 is mediated by a new family of HMTases without a SET domain. *Curr. Biol.* **12**, 1052-1058. doi:10.1016/S0960-9822(02)00901-6

Fonseca, N. A., Marioni, J. and Brazma, A. (2014). RNA-Seq gene profiling - a systematic empirical comparison. *PLoS ONE* **9**, e107026. doi:10.1371/journal.pone.0107026

Gallardo, T., Shirley, L., John, G. B. and Castrillon, D. H. (2007). Generation of a germ cell-specific mouse transgenic Cre line, Vasa-Cre. *Genesis* **45**, 413-417. doi:10.1002/dvg.20310

Gaucher, J., Reynoird, N., Montellier, E., Boussouar, F., Rousseaux, S. and Khochbin, S. (2010). From meiosis to postmeiotic events: the secrets of histone disappearance. *FEBS J.* **277**, 599-604. doi:10.1111/j.1742-4658.2009.07504.x

Gaucher, J., Boussouar, F., Montellier, E., Curtet, S., Buchou, T., Bertrand, S., Hery, P., Jounier, S., Depaux, A., Vitte, A.-L. et al. (2012). Bromodomain-dependent stage-specific male genome programming by Brdt. *EMBO J.* **31**, 3809-3820. doi:10.1038/emboj.2012.233

Goudarzi, A., Zhang, D., Huang, H., Barral, S., Kwon, O. K., Qi, S., Tang, Z., Buchou, T., Vitte, A.-L., He, T. et al. (2016). Dynamic competing Histone H4 K5K8 acetylation and butyrylation are hallmarks of highly active gene promoters. *Mol. Cell* **62**, 169-180. doi:10.1016/j.molcel.2016.03.014

Govin, J., Escoffier, E., Rousseaux, S., Kuhn, L., Ferro, M., Thévenon, J., Catena, R., Davidson, I., Garin, J., Khochbin, S. et al. (2007). Pericentric heterochromatin reprogramming by new histone variants during mouse spermiogenesis. *J. Cell Biol.* **176**, 283-294. doi:10.1083/jcb.200604141

Green, C. D., Ma, Q., Manske, G. L., Shami, A. N., Zheng, X., Marini, S., Moritz, L., Sultan, C., Gurczynski, S. J., Moore, B. B. et al. (2018). A comprehensive roadmap of murine spermatogenesis defined by single-cell RNA-seq. *Dev. Cell* **46**, 651-667.e10. doi:10.1016/j.devcel.2018.07.025

Guenther, M. G., Lawton, L. N., Rozovskaia, T., Frampton, G. M., Levine, S. S., Volkert, T. L., Croce, C. M., Nakamura, T., Canaani, E. and Young, R. A. (2008). Aberrant chromatin at genes encoding stem cell regulators in human mixed-lineage leukemia. *Genes Dev.* **22**, 3403-3408. doi:10.1101/gad.1741408

Haaf, T. and Ward, D. C. (1995). Higher order nuclear structure in mammalian sperm revealed by in situ hybridization and extended chromatin fibers. *Exp. Cell Res.* **219**, 604-611. doi:10.1006/excr.1995.1270

Hao, Y., Hao, S., Andersen-Nissen, E., Mauck, W. M., Zheng, S., Butler, A., Lee, M. J., Wilk, A. J., Darby, C., Zager, M. et al. (2021). Integrated analysis of multimodal single-cell data. *Cell* **184**, 3573-3587.e29. doi:10.1016/j.cell.2021.04.048

Hazzouri, M., Pivot-Pajot, C., Faure, A.-K., Usson, Y., Pelletier, R., Sèle, B., Khochbin, S. and Rousseaux, S. (2000). Regulated hyperacetylation of core histones during mouse spermatogenesis: involvement of histone-deacetylases. *Eur. J. Cell Biol.* **79**, 950-960. doi:10.1078/0171-9335-00123

Hermann, B. P., Cheng, K., Singh, A., Roa-De La Cruz, L., Mutoji, K. N., Chen, I.-C., Gildersleeve, H., Lehle, J. D., Mayo, M., Westernströer, B. et al. (2018). The mammalian spermatogenesis single-cell transcriptome, from spermatogonial stem cells to spermatids. *Cell Rep.* **25**, 1650-1667.e8. doi:10.1016/j.celrep.2018.10.026

Hermo, L., Pelletier, R.-M., Cyr, D. G. and Smith, C. E. (2010). Surfing the wave, cycle, life history, and genes/proteins expressed by testicular germ cells. Part 1: background to spermatogenesis, spermatogonia, and spermatocytes. *Microsc. Res. Tech.* **73**, 241-278. doi:10.1002/jemt.20783

Hoghoughi, N., Barral, S., Curtet, S., Chuffart, F., Charbonnier, G., Puthier, D., Buchou, T., Rousseaux, S. and Khochbin, S. (2020). RNA-guided genomic localization of H2A.L.2 histone variant. *Cells* **9**, 474. doi:10.3390/cells9020474

Hu, Y.-C., de Rooij, D. G. and Page, D. C. (2013). Tumor suppressor gene Rb is required for self-renewal of spermatogonial stem cells in mice. *Proc. Natl. Acad. Sci. USA* **110**, 12685-12690. doi:10.1073/pnas.1311548110

Jones, B., Su, H., Bhat, A., Lei, H., Bajko, J., Hevi, S., Baltus, G. A., Kadam, S., Zhai, H., Valdez, R. et al. (2008). The histone H3K79 methyltransferase Dot1L is essential for mammalian development and heterochromatin structure. *PLoS Genet.* **4**, e1000190. doi:10.1371/journal.pgen.1000190

Jonkers, I., Kwak, H. and Lis, J. T. (2014). Genome-wide dynamics of Pol II elongation and its interplay with promoter proximal pausing, chromatin, and exons ed. K. Struhl. *eLife* **3**, e02407. doi:10.7554/eLife.02407

Kari, V., Raul, S. K., Henck, J. M., Kitz, J., Kramer, F., Kosinsky, R. L., Übelmesser, N., Mansour, W. Y., Eggert, J., Spitzner, M. et al. (2019). The histone methyltransferase DOT1L is required for proper DNA damage response, DNA repair, and modulates chemotherapy responsiveness. *Clin. Epigenet.* **11**, 4. doi:10.1186/s13148-018-0601-1

Kim, S.-K., Jung, I., Lee, H., Kang, K., Kim, M., Jeong, K., Kwon, C. S., Han, Y.-M., Kim, Y. S., Kim, D. et al. (2012). Human histone H3K79 methyltransferase DOT1L protein [corrected] binds actively transcribing RNA polymerase II to regulate gene expression. *J. Biol. Chem.* **287**, 39698-39709. doi:10.1074/jbc.M112.384057

Korsunsky, I., Millard, N., Fan, J., Slowikowski, K., Zhang, F., Wei, K., Baglaenko, Y., Brenner, M., Loh, P.-R. and Raychaudhuri, S. (2019). Fast, sensitive and accurate integration of single-cell data with Harmony. *Nat. Methods* **16**, 1289-1296. doi:10.1038/s41592-019-0619-0

Kotaja, N., Kimmins, S., Brancorsini, S., Hentsch, D., Vonesch, J.-L., Davidson, I., Parvinen, M. and Sassone-Corsi, P. (2004). Preparation, isolation and characterization of stage-specific spermatogenic cells for cellular and molecular analysis. *Nat. Methods* **1**, 249-254. doi:10.1038/nmeth1204-249

La Spina, F. A., Romanato, M., Brugo-Olmedo, S., De Vincentiis, S., Julianelli, V., Rivera, R. M. and Buffone, M. G. (2014). Heterogeneous distribution of

histone methylation in mature human sperm. *J. Assist. Reprod. Genet.* **31**, 45-49. doi:10.1007/s10815-013-0137-4
Lacoste, N., Utley, R. T., Hunter, J. M., Poirier, G. G. and Côté, J. (2002). Disruptor of Telomeric Silencing-1 Is a Chromatin-specific Histone H3 Methyltransferase. *J. Biol. Chem.* **277**, 30421-30424. doi:10.1074/jbc.C200366200
Law, N. C. and Oatley, J. M. (2020). Developmental underpinnings of spermatogonial stem cell establishment. *Andrology* **8**, 852-861. doi:10.1111/andr.12810
Leblond, C. P. and Clermont, Y. (1952). Definition of the stages of the cycle of the seminiferous epithelium in the rat. *Ann. N. Y. Acad. Sci.* **55**, 548-573. doi:10.1111/j.1749-6632.1952.tb26576.x
Leduc, F., Maquennehan, V., Nkoma, G. B. and Boissonneault, G. (2008). DNA damage response during chromatin remodeling in elongating spermatids of mice1. *Biol. Reprod.* **78**, 324-332. doi:10.1095/biolreprod.107.064162
Lewis, J. D., Song, Y., de Jong, M. E., Bagha, S. M. and Ausió, J. (2003). A walk though vertebrate and invertebrate protamines. *Chromosoma* **111**, 473-482. doi:10.1007/s00412-002-0226-0
Li, W., Wu, J., Kim, S.-Y., Zhao, M., Hearn, S. A., Zhang, M. Q., Meistrich, M. L. and Mills, A. A. (2014). Chd5 orchestrates chromatin remodelling during sperm development. *Nat. Commun.* **5**, 3812. doi:10.1038/ncomms4812
Lin, H., Cheng, K., Kubota, H., Lan, Y., Riedel, S. S., Kakiuchi, K., Sasaki, K., Bernt, K. M., Bartolomei, M. S., Luo, M. et al. (2022). Histone methyltransferase DOT1L is essential for self-renewal of germline stem cells. *Genes Dev.* **36**, 752-763. doi:10.1101/gad.349550.122
Lin, H., Cossu, I. G., Leu, N. A., Deshpande, A. J., Bernt, K. M., Luo, M. and Wang, P. J. (2023). The DOT1L-MLLT10 complex regulates male fertility and promotes histone removal during spermiogenesis. *Development* **150**, dev201501. doi:10.1242/dev.201501
Luense, L. J., Donahue, G., Lin-Shiao, E., Rangel, R., Weller, A. H., Bartolomei, M. S. and Berger, S. L. (2019). Gcn5-mediated histone acetylation governs nucleosome dynamics in spermiogenesis. *Dev. Cell* **51**, 745-758.e6. doi:10.1016/j.devcel.2019.10.024
Lukassen, S., Bosch, E., Ekici, A. B. and Winterpacht, A. (2018). Characterization of germ cell differentiation in the male mouse through single-cell RNA sequencing. *Sci. Rep.* **8**, 6521. doi:10.1038/s41598-018-24725-0
Malla, A. B., Yu, H., Kadimi, S., Lam, T., Cox, A. L., Smith, Z. D. and Lesch, B. J. (2021). *DOT1L bridges transcription and heterochromatin formation at pericentromeres. bioRxiv* https://www.biorxiv.org/content/10.1101/2021.10.21.465349v1
Meistrich, M. L., Trostle-Weige, P. K., Lin, R., Allis, C. D. and Bhatnagar, Y. M. (1992). Highly acetylated H4 is associated with histone displacement in rat spermatids. *Mol. Reprod. Dev.* **31**, 170-181. doi:10.1002/mrd.1080310303
Meistrich, M. L., Mohapatra, B., Shirley, C. R. and Zhao, M. (2003). Roles of transition nuclear proteins in spermiogenesis. *Chromosoma* **111**, 483-488. doi:10.1007/s00412-002-0227-z
Mele, M., Ferreira, P. G., Reverter, F., DeLuca, D. S., Monlong, J., Sammeth, M., Young, T. R., Goldmann, J. M., Pervouchine, D. D., Sullivan, T. J. et al. (2015). Human genomics. The human transcriptome across tissues and individuals. *Science* **348**, 660-665. doi:10.1126/science.aaa0355
Merges, G. E., Meier, J., Schneider, S., Kruse, A., Fröbius, A. C., Kirfel, G., Steger, K., Arévalo, L. and Schorle, H. (2022). Loss of Prm1 leads to defective chromatin protamination, impaired PRM2 processing, reduced sperm motility and subfertility in male mice. *Development* **149**, dev200330. doi:10.1242/dev.200330
Meyer, R. G., Ketchum, C. C. and Meyer-Ficca, M. L. (2017). Heritable sperm chromatin epigenetics: a break to remember. *Biol. Reprod.* **97**, 784-797. doi:10.1093/biolre/iox137
Meyer-Ficca, M., Müller-Navia, J. and Scherthan, H. (1998). Clustering of pericentromeres initiates in step 9 of spermiogenesis of the rat (Rattus norvegicus) and contributes to a well defined genome architecture in the sperm nucleus. *J. Cell Sci.* **111**, 1363-1370. doi:10.1242/jcs.111.10.1363
Mohan, M., Herz, H.-M., Takahashi, Y.-H., Lin, C., Lai, K. C., Zhang, Y., Washburn, M. P., Florens, L. and Shilatifard, A. (2010). Linking H3K79 trimethylation to Wnt signaling through a novel Dot1-containing complex (DotCom). *Genes Dev.* **24**, 574-589. doi:10.1101/gad.1898410
Morinière, J., Rousseaux, S., Steuerwald, U., Soler-López, M., Curtet, S., Vitte, A.-L., Govin, J., Gaucher, J., Sadoul, K., Hart, D. J. et al. (2009). Cooperative binding of two acetylation marks on a histone tail by a single bromodomain. *Nature* **461**, 664-668. doi:10.1038/nature08397
Ng, H. H., Feng, Q., Wang, H., Erdjument-Bromage, H., Tempst, P., Zhang, Y. and Struhl, K. (2002). Lysine methylation within the globular domain of histone H3 by Dot1 is important for telomeric silencing and Sir protein association. *Genes Dev.* **16**, 1518-1527. doi:10.1101/gad.1001502
Niedenberger, B. A., Busada, J. T. and Geyer, C. B. (2015). Marker expression reveals heterogeneity of spermatogonia in the neonatal mouse testis. *Reproduction* **149**, 329-338. doi:10.1530/REP-14-0653
Oakberg, E. F. (1956). A description of spermiogenesis in the mouse and its use in analysis of the cycle of the seminiferous epithelium and germ cell renewal. *Am. J. Anat.* **99**, 391-413. doi:10.1002/aja.1000990303
Okada, Y., Scott, G., Ray, M. K., Mishina, Y. and Zhang, Y. (2007). Histone demethylase JHDM2A is critical for Tnp1 and Prm1 transcription and spermatogenesis. *Nature* **450**, 119-123. doi:10.1038/nature06236
Oliva, R. (2006). Protamines and male infertility. *Hum. Reprod. Update* **12**, 417-435. doi:10.1093/humupd/dml009
Ontoso, D., Acosta, I., van Leeuwen, F., Freire, R. and San-Segundo, P. A. (2013). Dot1-dependent histone H3K79 methylation promotes activation of the Mek1 meiotic checkpoint effector kinase by regulating the Hop1 adaptor. *PLoS Genet.* **9**, e1003262. doi:10.1371/journal.pgen.1003262
Ooga, M., Inoue, A., Kageyama, S.-I., Akiyama, T., Nagata, M. and Aoki, F. (2008). Changes in H3K79 methylation during preimplantation development in mice. *Biol. Reprod.* **78**, 413-424. doi:10.1095/biolreprod.107.063453
Ooga, M., Suzuki, M. G. and Aoki, F. (2013). Involvement of DOT1L in the remodeling of heterochromatin configuration during early preimplantation development in mice. *Biol. Reprod.* **89**, 145, 1-10. doi:10.1095/biolreprod.113.113258
Papatheodorou, I., Moreno, P., Manning, J., Fuentes, A. M.-P., George, N., Fexova, S., Fonseca, N. A., Füllgrabe, A., Green, M., Huang, N. et al. (2020). Expression Atlas update: from tissues to single cells. *Nucleic Acids Res.* **48**, D77-D83. doi:10.1093/nar/gkz947
Peters, A. H. F. M., Plug, A. W., van Vugt, M. J. and de Boer, P. (1997). A drying-down technique for the spreading of mammalian meiocytes from the male and female germline. *Chromosome Res.* **5**, 66-68. doi:10.1023/A:1018445520117
Pivot-Pajot, C., Caron, C., Govin, J., Vion, A., Rousseaux, S. and Khochbin, S. (2003). Acetylation-dependent chromatin reorganization by BRDT, a testis-specific bromodomain-containing protein. *Mol. Cell. Biol.* **23**, 5354-5365. doi:10.1128/MCB.23.15.5354-5365.2003
Pogany, G. C., Corzett, M., Weston, S. and Balhorn, R. (1981). DNA and protein content of mouse sperm: implications regarding sperm chromatin structure. *Exp. Cell Res.* **136**, 127-136. doi:10.1016/0014-4827(81)90044-6
Prakash Yadav, R., Leskinen, S., Ma, L., Mäkelä, J.-A. and Kotaja, N. (2023). Chromatin remodelers HELLS, WDHD1 and BAZ1A are dynamically expressed during mouse spermatogenesis. *Reproduction* **165**, 49-63. doi:10.1530/REP-22-0240
Probst, A. V., Okamoto, I., Casanova, M., El Marjou, F., Le Baccon, P. and Almouzni, G. (2010). A strand-specific burst in transcription of pericentric satellites is required for chromocenter formation and early mouse development. *Dev. Cell* **19**, 625-638. doi:10.1016/j.devcel.2010.09.002
Qian, M.-X., Pang, Y., Liu, C. H., Haratake, K., Du, B.-Y., Ji, D.-Y., Wang, G.-F., Zhu, Q.-Q., Song, W., Yu, Y. et al. (2013). Acetylation-mediated proteasomal degradation of core histones during DNA repair and spermatogenesis. *Cell* **153**, 1012-1024. doi:10.1016/j.cell.2013.04.032
R Core Team. V Austria URL. https://www.R-project.org/. (2015). R: A language and environment for statistical computing. https://www.R-project.org/.
Ribas-Maynou, J., Nguyen, H., Wu, H. and Ward, W. S. (2022). Functional Aspects of Sperm Chromatin Organization. *Results Probl. Cell Differ.* **70**, 295-311. doi:10.1007/978-3-031-06573-6_10
Russell, L., Ettlin, R., Sinha Hikim, A. and Clegg, E. (1990). *Histological and Histopathological Evaluation of the Testis*. Clearwater, FL: Cache River Press.
Saksouk, N., Simboeck, E. and Déjardin, J. (2015). Constitutive heterochromatin formation and transcription in mammals. *Epigenet. Chromatin* **8**, 3. doi:10.1186/1756-8935-8-3
Sasaki, K., Ito, T., Nishino, N., Khochbin, S. and Yoshida, M. (2009). Real-time imaging of histone H4 hyperacetylation in living cells. *Proc. Natl Acad. Sci. USA* **106**, 16257-16262. doi:10.1073/pnas.0902150106
Shang, E., Nickerson, H. D., Wen, D., Wang, X. and Wolgemuth, D. J. (2007). The first bromodomain of Brdt, a testis-specific member of the BET sub-family of double-bromodomain-containing proteins, is essential for male germ cell differentiation. *Development* **134**, 3507-3515. doi:10.1242/dev.004481
Shiota, H., Barral, S., Buchou, T., Tan, M., Couté, Y., Charbonnier, G., Reynoird, N., Boussouar, F., Gérard, M., Zhu, M. et al. (2018). Nut directs p300-dependent, genome-wide H4 hyperacetylation in male germ cells. *Cell Rep.* **24**, 3477-3487.e6. doi:10.1016/j.celrep.2018.08.069
Shirley, C. R., Hayashi, S., Mounsey, S., Yanagimachi, R. and Meistrich, M. L. (2004). Abnormalities and reduced reproductive potential of sperm from Tnp1- and Tnp2-null double mutant mice1. *Biol. Reprod.* **71**, 1220-1229. doi:10.1095/biolreprod.104.029363
Steger, D. J., Lefterova, M. I., Ying, L., Stonestrom, A. J., Schupp, M., Zhuo, D., Vakoc, A. L., Kim, J.-E., Chen, J., Lazar, M. A. et al. (2008). DOT1L/KMT4 recruitment and H3K79 methylation are ubiquitously coupled with gene transcription in mammalian cells. *Mol. Cell. Biol.* **28**, 2825-2839. doi:10.1128/MCB.02076-07
Thul, P. J., Åkesson, L., Wiking, M., Mahdessian, D., Geladaki, A., Ait Blal, H., Alm, T., Asplund, A., Björk, L., Breckels, L. M. et al. (2017). A subcellular map of the human proteome. *Science* **356**, eaal3321. doi:10.1126/science.aal3321
Uhlén, M., Fagerberg, L., Hallström, B. M., Lindskog, C., Oksvold, P., Mardinoglu, A., Sivertsson, Å., Kampf, C., Sjöstedt, E., Asplund, A. et al. (2015). Proteomics. Tissue-based map of the human proteome. *Science* **347**, 1260419. doi:10.1126/science.1260419

van Leeuwen, F., Gafken, P. R. and Gottschling, D. E. (2002). Dot1p modulates silencing in yeast by methylation of the nucleosome core. *Cell* **109**, 745-756. doi:10.1016/S0092-8674(02)00759-6

Velazquez Camacho, O., Galan, C., Swist-Rosowska, K., Ching, R., Gamalinda, M., Karabiber, F., De La Rosa-Velazquez, I., Engist, B., Koschorz, B., Shukeir, N. et al. (2017). Major satellite repeat RNA stabilize heterochromatin retention of Suv39h enzymes by RNA-nucleosome association and RNA:DNA hybrid formation. *eLife* **6**, e25293. doi:10.7554/eLife.25293

Veloso, A., Kirkconnell, K. S., Magnuson, B., Biewen, B., Paulsen, M. T., Wilson, T. E. and Ljungman, M. (2014). Rate of elongation by RNA polymerase II is associated with specific gene features and epigenetic modifications. *Genome Res.* **24**, 896-905. doi:10.1101/gr.171405.113

Wang, T., Gao, H., Li, W. and Liu, C. (2019). Essential role of histone replacement and modifications in male fertility. *Front. Genet.* **10**, 962. doi:10.3389/fgene.2019.00962. https://www.frontiersin.org/articles/10.3389/fgene.2019.00962 (Accessed November 4, 2022).

Wood, K., Tellier, M. and Murphy, S. (2018). DOT1L and H3K79 methylation in transcription and genomic stability. *Biomolecules* **8**, 11. doi:10.3390/biom8010011

Yadav, R. P., Mäkelä, J.-A., Hyssälä, H., Cisneros-Montalvo, S. and Kotaja, N. (2020). DICER regulates the expression of major satellite repeat transcripts and meiotic chromosome segregation during spermatogenesis. *Nucleic Acids Res.* **48**, 7135-7153. doi:10.1093/nar/gkaa460

Yeh, Y.-H., Hu, M., Nakagawa, T., Sakashita, A., Yoshida, S., Maezawa, S. and Namekawa, S. H. (2021). Isolation of murine spermatogenic cells using a violet-excited cell-permeable DNA binding dye. *J. Vis. Exp.* **167**, doi:10.3791/61666

Zhao, M., Shirley, C. R., Hayashi, S., Marcon, L., Mohapatra, B., Suganuma, R., Behringer, R. R., Boissonneault, G., Yanagimachi, R. and Meistrich, M. L. (2004a). Transition nuclear proteins are required for normal chromatin condensation and functional sperm development. *Genesis* **38**, 200-213. doi:10.1002/gene.20019

Zhao, M., Shirley, C. R., Mounsey, S. and Meistrich, M. L. (2004b). Nucleoprotein transitions during spermiogenesis in mice with transition nuclear protein Tnp1 and Tnp2 mutations. *Biol. Reprod.* **71**, 1016-1025. doi:10.1095/biolreprod.104.028191

Zhuang, T., Hess, R. A., Kolla, V., Higashi, M., Raabe, T. D. and Brodeur, G. M. (2014). CHD5 is required for spermiogenesis and chromatin condensation. *Mech. Dev.* **131**, 35-46. doi:10.1016/j.mod.2013.10.005